José João Henriques
Ministro

# Um estudo sobre a síntese e as propriedades ópticas de *quantum dots* de InP

# A study on the synthesis and the optical properties of InP-based quantum dots

UNIVERSITEIT GENT

FACULTY OF SCIENCES

Department of Inorganic and Physical Chemistry
Physics and Chemistry of Nanostructures Group

# A study on the synthesis and the optical properties of InP-based quantum dots

Thesis submitted to obtain
the degree of Master of Science in Chemistry by

José Ministro

Academic year 2013 - 2014

Promoter: prof. dr. ir. Zeger Hens
Supervisors: Sofie Abé and Dr. Mickaël Tessier

# Acknowledgements

Writing these last pages of my thesis manuscript means all the rest is (finally!) written. But it means as well that this thrilling adventure is coming to an end. It has been an exciting and eventful year that I will never forget and I am happy to have learned so much and to have met so many people.

Professor Zeger Hens, I want to thank you, first of all, for allowing me to come to the University of Ghent and work in your group. I am now sure that I couldn't have chosen a better place to do my thesis. You taught me a lot and I'm very thankful for all the passion and motivation that you conveyed to me and for always keeping my thesis on a good track.

I want to thank my dear supervisors Sofie Abé and Mickaël Tessier. Sofie, thanks for your infinite availability, patience and support. You were a true mentor from the very beginning and it was really a pleasure to learn and work with you. Mickaël, you arrived after me, but soon you became essential to my thesis work. Thank you for the constant orientation, explanations and suggestions that were crucial for the end result of my thesis.

I also want to acknowledge all the members of PCN group. Thank you all for making this year so enjoyable, for all the enlightening discussions during our meetings and your always pertinent suggestions and advice. In particular, thank you Kim for the NMR measurements, for your valuable observations, and for making the lab such a fun place to work. Thank you Jonathan for the several discussions on InP reactions, "unreactions" and all kind of things happening inside a 3-neck flask. Thank you Ruben for the XRD measurements and Dorian for the samples and results you provided me. Elleke van Harten and Karel Lambert, although I haven't personally met you, your InP samples and spectra (and your reports on that) were essential for my results. Thank you.

There were some persons who enabled this thesis to become far more complete and allowed to me to get in touch with a whole new range of techniques. Thank you Professor Philippe Smet and Jonas Joos for your help with the time-resolved PL measurements and with the data processing. I want to express my gratitude to Dr. Lieve Balcaen, Dr. Els Bruneel and Qiang Zhao for the ICP-OES, XPS and RBS measurements.

I also want to thank my Erasmus friends who made this year really memorable. Thanks for all the shared laughs, dinners, trips, study groups, parties and so much more and for cheering me up whenever I was going nuts.

This thesis does not only mark the end of one great year, but also of four unforgettable years in the University of Aveiro. During my academic path I have met a lot of truly inspiring and brilliant people. I cannot thank them all but there are some I really must acknowledge, for several reasons. Professors Armando Silvestre, Artur Silva, João Rocha, Paulo Claro and Tito Trindade, thank you for being a source of motivation, enthusiasm, knowledge and advice. It was a pleasure to work with you.

These last five years were undoubtedly the best of my life and a great part of it is due to all the many and great friends I made, to whom I am very grateful. I can't, however, mention them all without risking largely exceeding the limit of pages of this manuscript and still forget some.

Finally, I would like to thank my family, the best I could have, for always being there for me. Despite the distance (*e das saudades*), you were always close.

And now excuse me, but this is for the best of the best…

Obrigado mãe e obrigado pai, por serem os melhores do mundo. Não há muito que eu consiga escrever para exprimir o que verdadeiramente sinto. Se hoje sou o que sou, devo-o inteiramente a vocês e ao exemplo que sempre representaram. Obrigado por tudo o que me proporcionaram e pelo apoio incondicional em todas as ocasiões. Obrigado Joana, por seres a melhor irmã mais velha (apesar de a única). És uma inspiração e a tua confiança em mim significa muito. E obrigado Rute, meu porto de abrigo, tão longe mas sempre perto, por me aturares e reconfortares como só tu sabes. Simplesmente, amo-vos.

José Ministro

Ghent, June 5th 2014

# English summary

The aim of this work is the study of the optical properties of InP quantum dots (QDs) and the exploration of a new method for the synthesis of InP/CdS core-shell QDs.

A multitude of research on colloidal QDs requires detailed knowledge of the relation between optical and structural properties, namely the sizing curve, the intrinsic absorption coefficient and the molar extinction coefficient. In this work, InP QDs were synthesized and structurally and optically characterized. The sizing curve was established from the average QD diameter, obtained by transmission electron microscopy, and the position of the first excitonic absorption peak. The intrinsic absorption coefficient and molar extinction coefficient were determined from quantitative elemental analysis and the absorbance of the nanocrystals at short wavelengths. We found that the intrinsic absorption coefficient is size-independent in this wavelength region and the molar extinction coefficient increases linearly with the QD volume.

The focus of our study was then shifted to the fabrication of core-shell QD hetero-structures, based on a recently reported method that used a more sustainable and much cheaper phosphorus precursor for the synthesis of high-quality InP/ZnS QDs. Using this procedure, we synthesized highly luminescent InP/CdS QDs and their emission could be tuned in the visible and near-infrared spectral regions. Furthermore, time-resolved photo-luminescence measurements were performed on samples of InP/ZnS and InP/CdS QDs.

We also report an exploratory study on the mechanism of formation of InP QDs with this new method. A thorough understanding of the reaction mechanism will enable a better control over the synthesis products and is potentially relevant for the fabrication of QDs consisting of other III-V semiconductors (e.g. GaP).

# Nederlandstalige samenvatting

Het doel van dit werk is de studie van de optische eigenschappen van InP kwantum dots (QDs) en de exploratie van een nieuwe methode voor de synthese van InP/CdS kern-schil (core-shell) QDs.

Onderzoek naar colloïdale QDs vereist een gedetailleerde kennis van het verband tussen optische en structurele eigenschappen: een relatie tussen de energie van de verboden zone en diameter van de QD (dimensioneringscurve), de intrinsieke absorptiecoëfficiënt en de molaire extinctiecoëfficiënt. In dit werk werden InP QDs gesynthetiseerd en gekarakteriseerd, zowel structureel als optisch. De dimensioneringscurve werd opgesteld op basis van de gemiddelde QD diameter, verkregen door transmissie-elektronenmicroscopie en de locatie van de eerste excitonpiek in het absorptiespectrum. De intrinsieke absorptiecoëfficiënt en de molaire extinctiecoëfficiënt werden bepaald via kwantitatieve elementaire analyse en de absorptie van de nanokristallen bij korte golflengten. We toonden aan dat de intrinsieke absorptiecoëfficiënt diameter-onafhankelijk is in dit golflengtegebied en dat de molaire extinctiecoëfficiënt lineair toeneemt met de hoeveelheid halfgeleidermateriaal.

De focus van onze studie werd vervolgens verschoven naar de synthese van core-shell QD heterostructuren, gebaseerd op een recent ontwikkelde methode voor de synthese van hoogwaardige InP/ZnS QDs die een duurzamere en goedkopere fosforprecursor gebruikt. Zodoende hebben we hoog luminescente InP/CdS QDs gesynthetiseerd, waarvan de emissie kan gevarieerd worden in de zichtbare en nabij-infrarode spectrale gebieden. Verder werden metingen van het verval van de fotoluminescentie uitgevoerd op InP/ZnS en InP/CdS QDs.

Tenslotte werd een verkennende studie uitgevoerd over het mechanisme van de synthese van InP QDs met deze nieuwe methode. Een goed begrip van het reactiemechanisme is van belang voor een betere controle over de syntheseproducten en kan tevens de vervaardiging van QDs bestaande uit andere type III-V halfgeleiders, bijv. GaP, mogelijk maken.

# Contents

# List of abbreviations

| | |
|---|---|
| DDT | 1-dodecanethiol |
| FWHM | Full width at half maximum |
| HWHM | Half width at half maximum |
| ICP-OES | Inductively coupled plasma optical emission spectrometry |
| MA | Myristic acid |
| NIR | Near-infrared |
| NMR | Nuclear magnetic resonance |
| ODE | 1-Octadecene |
| OLA | Oleylamine |
| $P(DMA)_3$ | Tris(dimethylamino)phosphine |
| $P(TMS)_3$ | Tris(trimethylsilyl)phosphine |
| PL | Photoluminescence |
| PLQY | Photoluminescence quantum yield |
| QD(s) | Quantum dot(s) |
| RBS | Rutherford backscattering spectrometry |
| rpm | Revolutions per minute |
| RSD | Relative standard deviation |
| UV | Ultraviolet |
| UV-vis | Ultraviolet-visible |
| TEM | Transmission electron microscopy |
| TOPS | Tri-n-octylphosphine sulphide |
| XPS | X-ray photoelectron spectroscopy |
| XRD | X-ray diffraction |

# List of symbols

| | |
|---|---|
| $A$ | Absorbance |
| $N_A$ | Avogadro's number |
| $E_g$ | Band gap energy |
| $d_{QD}$ | Diameter of quantum dots |
| $R_{In/P}$ | Indium-to-phosphorus ratio |
| $\mu_i$ | Intrinsic absorption coefficient |
| $\tau$ | Lifetime |
| $f_{LF}$ | Local field factor |
| $\varepsilon_\lambda$ | Molar extinction coefficient (at wavelength $\lambda$) |
| $V_m$ | Molar volume |
| $L$ | Path length |
| $h$ | Planck's constant |
| $^1$H | Proton |
| $\sigma_d$ | Size dispersion |
| $c$ | Speed of light in vacuum |
| $f$ | Volume fraction |
| $\lambda$ | Wavelength |
| $\lambda_{1S-1S}$ | Wavelength of the first excitonic absorption peak maximum |

# Chapter 1. Introduction

## 1.1. Why go small?

According to the American Society for Testing and Materials, nanotechnology refers to "a wide range of technologies that measure, manipulate, or incorporate materials and/or features with at least one dimension between approximately 1 and 100 nm. Such applications exploit those properties, distinct from bulk or molecular systems, of nanoscale components.".[1] The interest of fabricating materials within the nanoscale is thus not only related to the manufacturing of smaller sized devices. Nanomaterials show different properties from their bulk counterparts, such as mechanical, magnetic, optical or electrical properties[2] and open up new worlds for interactions that were not available otherwise, for instance, with biological systems.[3] Nanotechnology is therefore regarded as a cutting-edge research field with applications in areas as distinct as food technology, automobile and aerospace engineering, textile and environmental industries or healthcare.[4]

Nanostructured materials can be so different that it is not always easy to classify them, but some general classes can be established, some of the more common being semiconductor nanoparticles, metal nanoparticles, nanoceramics (nanosized metal oxides) and carbon nanostructures. Colloidal semiconductor nanoparticles, usually referred to as quantum dots (QDs), are the nanomaterials that are in the focus of this thesis.

## 1.2. Quantum dots

The absorption of a photon by a semiconductor material creates a quasiparticle, called an exciton, which is a bound state between the electron promoted to the conduction band and the vacancy (or hole) in the valence band left behind by that electron. The distance between these two charge carriers is called the exciton Bohr radius and it is characteristic of each bulk semiconductor material.

QDs exhibit quantum confinement of the charge carriers in the three dimensions of space, meaning that, as their radii get smaller than the exciton Bohr radius, confinement begins to affect the exciton wavefunction. This results in an increase of the band gap and

the appearance of discrete energy levels near the band edges with decreasing QD size.[5] Hence, it is possible to modify the band gap energy simply by varying the size of these nanoparticles, i.e., QDs have size-dependent optical properties, as light absorption and emission. This phenomenon can be observed in Figure 1a, where suspensions of colloidal CdSe QDs with different sizes are shown. Smaller QDs present a larger band gap and emit blue light, whereas an increasing diameter causes a red shift of the emission.

In addition to the increasing band gap energy, the QD size reduction also changes the energy band structure from the continuous nature of bulk semiconductors, to being quantized at the band edge. Therefore, distinct sharp peaks are detected in the absorption spectra of the QDs (Figure 1b), which are generally not seen in the absorption spectra of bulk semiconductors.

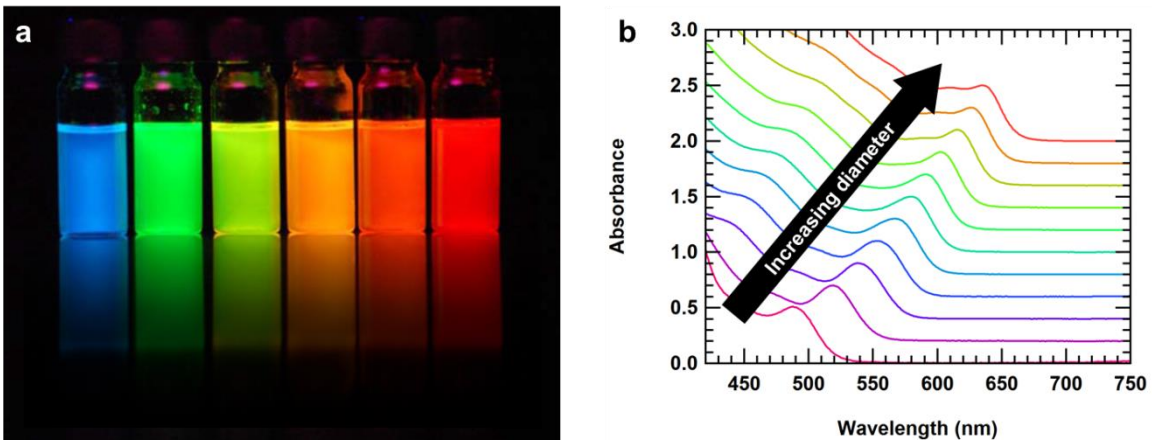


Figure 1. (a) Suspensions of CdSe QDs with diameters between 2 nm (left) and 6 nm (right) under UV light. Adapted from Lambert (2011).[6] (b) Absorption spectra of aliquots taken at different times during the synthesis of CdSe QDs. The spectra were shifted vertically for clarity.

High-quality QDs can present extremely high photoluminescence quantum yields (PLQYs) and photostability. They also exhibit narrow and symmetrical emission and very broad absorption, which enables them to be excited at any energy higher than their band gap. Different semiconductor materials have characteristic band gap energies and therefore QDs are optically active in a wide spectral range, from the ultraviolet to the near-infrared region.[7-8]

Applications of this class of nanomaterials are varied, with three of the most promising possibly being biological imaging, photovoltaic devices, and light-emitting

devices.[8] Currently, there are already QD-containing products available in the market, like the "QD kits" sold by Sigma Aldrich,[9] that are useful for researchers in biological and biomedical fields, and electronic devices, like in some models of televisions commercialised by Sony.[10]

For these two examples, QDs are handled either in water solution or in the form of thin films and, for that reason, a common requirement for their extended use is their flexibility in post-synthetic processing. This can generally be achieved with the synthesis of colloidal QDs by wet chemical routes.

## 1.3. Colloidal synthesis

Different synthesis strategies for the fabrication of QDs have been reported, based on both top-down and bottom-up approaches.[11] Colloidal synthesis of QDs presents several advantages, such as ease and low cost, and a high control over the QD shape, size and dispersity.[12] The hot-injection synthesis method, firstly reported by Murray et al. in 1993,[13] is nowadays used (with modifications) for the synthesis of an extensive range of QDs due to the high-quality of the obtained particles. This method generally consists of injecting one of the precursors in a hot reaction mixture (Figure 2) containing the other precursor and coordinating ligands in a non-coordinating solvent. This leads to the thermal decomposition of the precursors that react to form a solute or monomer, followed by the nucleation and growth of QDs.[14]

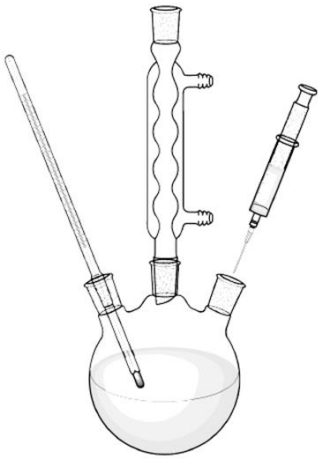

Figure 2. Schematic representation of the experimental set-up used in the hot-injection synthesis. A 3-neck flask is used to enable precursor injection, temperature control and an inert atmosphere.

## 1.4. Core-shell quantum dot heterostructures

Unlike their bulk counterparts, QDs have a huge surface area-to-volume ratio, and a very high amount of their atoms are located on the QD surface, meaning that surface effects have a large impact on the physics and chemistry of QDs. A frequent drawback with surface atoms is their inefficient passivation by the organic ligands, resulting in surface defects that form the so-called trap states. These are energy levels located inside the band gap that serve as channels for non-radiative exciton recombination or result in emission at lower wavelengths, consequently lowering the band-edge emission.

One solution for this problem is the epitaxial growth of a shell of another semiconductor material around each QD. This not only inhibits trap emission, increasing the PLQY of the nanocrystals, but also creates a physical barrier between the optically active core QD and the surrounding medium and provides a different means for tuning the optoelectronic properties of QDs beyond core size effects.[15] Depending on the band alignment between the core and the shell material, two major categories of core-shell heterostructures can be defined: type-I and type-II (Figure 3).

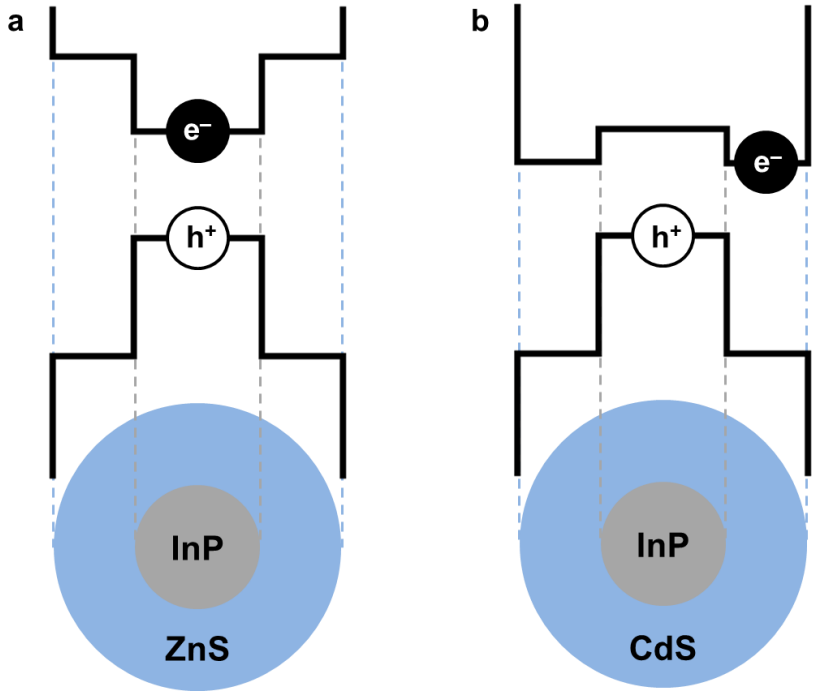


Figure 3. Alignment of the conduction and valence band edges for (a) type-I and (b) type-II heterostructures.

In type-I structures, the conduction and valence band edges of the core and the shell materials have a straddling configuration, i.e., the band gap of the shell material encompasses the one from the core, as shown in Figure 3a. The exciton is confined in the core of the QD and so the emission energy is determined by its band gap. These heterostructures generally result in improved chemical stability of the core material and in an enhancement of the PLQY. A typical type-I system is InP/ZnS.[16]

Type-II heterostructures show a staggered configuration of the shell band edge either towards higher or lower potentials than the core band edge. This causes a spatial separation of the charge carriers, with one of them being confined in the core, whereas the other is located in the shell. Hence, the band-edge gap energy decreases and the exciton lifetime increases, due to a reduced probability of recombination. The emission wavelength in these structures can be tuned by varying both the core size and the shell thickness. InP/CdS QDs are an example of a type-II system.[17]

## 1.5. Indium phosphide-based quantum dots

Due to their unique optical and electronic properties, QDs have been extensively studied in the last decades, especially those from groups II-VI and IV-VI, such as CdSe and PbS.[2, 5, 8, 11] Nonetheless, the focus of QD research has recently shifted towards III-V semiconductors, for two main reasons. First, III-V materials have a more covalent character than the typically ionic II-VI and IV-VI materials, which results in enhanced optical stability and reduced toxicity. Furthermore, the exciton Bohr radii are much larger in the III-V than in the II-VI systems, leading to stronger size quantization effects.[7] The main drawback of III-V QDs concerns the synthesis of high-quality nanocrystals, which is rather challenging and has prevented a more widespread use of these materials.

Among all III-V semiconductors, InP QDs are particularly interesting. Bulk InP has a band gap of 1.35 eV (918 nm) and the emission of InP QDs can thus be tuned in the visible and near-infrared (NIR) spectral regions. Furthermore InP has a low intrinsic toxicity, compared to cadmium, lead or selenium, making these QDs much more suitable for biological applications and environmentally sustainable industrial applications. The main problem with this material is the difficulty in obtaining monodisperse nanocrystals, which results in broad emission peaks.[7]

Two general approaches have been mostly explored for the colloidal synthesis of high-quality InP QDs: Hot-injection (presented in section 1.3) and heating up techniques. The heating up synthesis differs from the former in that all the precursors are added to the reaction mixture at room temperature and are then rapidly heated, leading to the thermal decomposition of the precursors.

A hot-injection procedure reported in 2007 by Xie et al.[18] proved to be exceptionally attractive in the formation of monodisperse InP QDs. This method uses indium carboxylates and tris(trimethylsilyl)phosphine as precursors and 1-octadecene (ODE) and fatty amines as non-coordinating solvent and ligands, respectively. This strategy enables a good control over QD size and size dispersion, and shorter times (up to 1 h) and lower temperature (178 ºC) are needed for the QD growth, while previous methods involved the growth of QDs for several days at temperatures higher than 250 ºC.[19-20] A large number of the following reports on InP QDs rely on this method with some modifications.[21-25]

As-synthesized InP QDs show very poor luminescence, but this problem can be tackled by either etching procedures or the synthesis of core-shell heterostructures. Etching of the QDs, for instance, with hydrofluoric acid, removes phosphorus dangling bonds and increases the band-edge emission.[26] The formation of core-shell QDs was referred on section 1.4 and is used in this study to improve and tune the photoluminescence (PL) properties of InP QDs.

## 1.6. Outline of this thesis

The aim of this work is the study of the optical properties of InP QDs and the exploration of a new method for the synthesis of InP/CdS core-shell QDs. This report is divided in six chapters, containing an introduction, methods, three chapters of results and discussion, and a conclusion.

Chapter 2 presents a brief overview of the methods used to characterize the QDs and these are divided in structural, optical and elemental analyses. The specifications of the measurement setups are listed and the sample preparation procedures are explained.

In chapter 3, we describe a synthesis procedure of colloidal InP QDs and their full characterization. We investigate the basic optical properties – sizing curve, intrinsic

absorption coefficient and extinction molar coefficient – of InP QDs by combining optical spectroscopy and elemental analysis. The application of the calculated properties is exemplified in the study of several parameters of a QD sample.

Chapter 4 reports the applicability of a recently published and very promising one-pot synthesis method to produce high-quality InP/ZnS and InP/CdS QDs. A typical synthesis is described and the resulting QDs are optically and structurally characterized. Then, we focus on tuning the PL properties of InP/CdS QDs and on studying their PL kinetic profiles by time-resolved spectroscopy.

The method reported in chapter 4 is explored in chapter 5 and we attempt its application to the synthesis of other III-V QDs, namely GaP. We launch the basis for an in-depth study of this synthesis that will enable a thorough understanding of the reaction mechanism.

Finally, in chapter 6 the general conclusions of this thesis are drawn. We highlight the major findings, and discuss their relevance and implications on this research field, as well as their limitations, closing this report with some suggestions and prospects on future research.

# Chapter 2. Characterization methods

## 2.1. Structural analysis

### X-Ray Diffraction

X-Ray Diffraction (XRD) is used to investigate the crystalline properties of the QDs. The position of the peaks in a diffractogram yields information about the crystalline phase of the QDs, by comparison with a crystallographic database, and the peak width is inversely proportional to the nanocrystal size, according to the Scherrer equation.[27] The XRD samples were prepared by dropcasting a QD suspension on a glass plate and measurements were performed on a Bruker D8 Diffractometer equipped with a 40 kV 40mA source using Cu $K_\alpha$ ($\lambda$=1.54Å) radiation and a Lynx Eye linear detector.

### Transmission electron microscopy

QDs can be directly visualised by transmission electron microscopy (TEM). A transmission electron microscope generates an electron beam that is transmitted through the sample, creating an image with resolution up to 50 pm.[6] Such images provide a qualitative analysis on the morphology of the QDs.

The imaging of a large number of QDs enables the determination of their surface area and, assuming they are spherical, the calculation of the average diameter. This is done with the software ImageJ, where the particles are discriminated from the background by creating a thresholded image. In the case of InP QDs, due to an insufficient contrast, this is done manually, by drawing a line on the edge of each particle, and the thresholding results in a binary image where all the marked particles become black and the background becomes white. Because of the low contrast, the edge of the QDs is not always easily identified and this can increase the error of the diameter estimation. However, for each QD dispersion between 80 to more than 250 particles are analysed, and the determined average diameter should be a good estimation of the real QD diameter.

The samples were prepared by dropcasting a diluted dispersion of QDs on carbon coated copper grids. As the InP QDs are easily oxidized, the sample preparation was

performed just right before the measurement. Bright field TEM images were recorded using a $C_s$ corrected JEOL 2200-FS microscope.

**Nuclear magnetic resonance spectroscopy**

Solution nuclear magnetic resonance (NMR) spectroscopy is a powerful tool to study the ligands of QDs. A full structural analysis can be performed on the ligands capping the QD surface, as well as a distinction between free and bound ligands.

The $^1$H NMR spectrum of ligands bound to a QD is different from a spectrum of the free ligands in solution. First, the linewidth of the resonances corresponding to bound ligands is broader than that of the free species. This is because the linewidth depends on the tumbling rate of a molecule in solution and, as larger molecules tumble more slowly than smaller ones, the tumbling rate of the bound ligands is slower than that of the free ligands. Moreover, due to a change on the chemical environment, resonances of the bound ligands show an increased chemical shift, compared to the resonances of the free ligands.[28] Figure 4 displays the $^1$H NMR spectra of free oleic acid versus oleic acid bound to the surface of CdSe QDs, where this is clearly demonstrated.

In this thesis, $^1$H NMR is used to characterize the InP QD surface, by identifying and quantifying the capping ligands. Moreover, it is used to assess the purity of QD dispersions, by analysing whether free ligands are present in solution, and to follow an exchange process between two amine groups.

The NMR samples were dried by evaporating the original solvent and adding deuterated toluene (toluene-d8). All NMR experiments were performed at room temperature on a Bruker 500 MHz AVANCE III spectrometer generating a $^1$H frequency of 500.13 MHz, equipped with a 5mm BBI-z or a 5mm TXI-z probe.

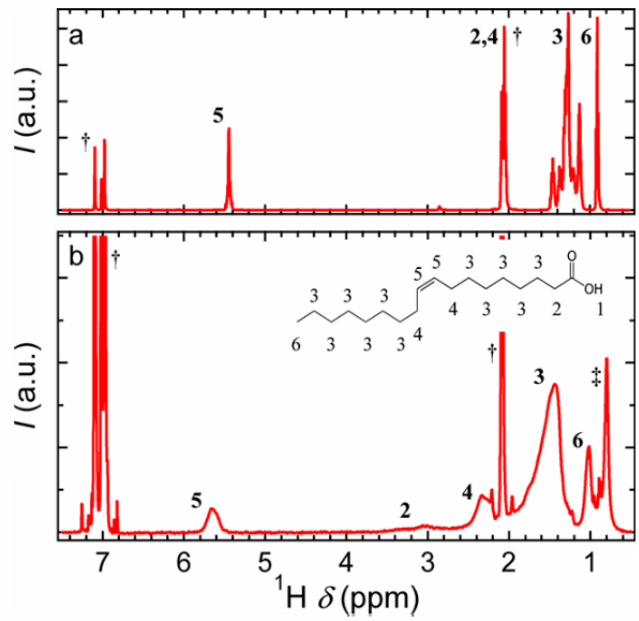


Figure 4. [1]H NMR spectrum of (a) oleic acid and (b) a QD dispersion of CdSe in toluene-d8. The labelled resonances are identified from 1 to 6 as (1-6) different oleic acid protons as indicated in the figure. † and ‡ indicate, respectively, resonances from residual solvent and water contamination. Reproduced from Zeger and Martins (2013).[28]

## 2.2. Optical analysis

### Ultraviolet-visible absorption spectroscopy

Ultraviolet-visible (UV-vis) absorption spectra of QD solutions are used to determine the QD diameter, the size dispersion and the concentration of semiconductor material and QDs.

As seen in Figure 2 (see section 1.2), the first excitonic absorption peak is shifted to longer wavelengths (red shifted) with increasing QD size and is broadened with increasing size dispersion. Therefore, the wavelength of the first excitonic absorption peak maximum $\lambda_{1S-1S}$ and the linewidth of this peak can be related, respectively, to the QD diameter and the size dispersion.

The absorption spectra of the QDs overlap at short wavelengths, regardless of the QD size, meaning that no quantum confinement effects are observed in this region and the absorption is size-independent. Hence, and according to the Lambert-Beer law, the QD

concentration can be calculated from the absorption values at short wavelengths, once the molar extinction coefficient is known. This will be further detailed in the next chapter.

The absorption spectra of QD dispersions were recorded using a Perkin Elmer Lambda 2 UV-vis spectrophotometer, using glass or quartz cuvettes with an optical path length of 1.00 cm.

**Photoluminescence spectroscopy**

Steady-state photoluminescence (PL) spectroscopy is used to study the radiative emission of the QDs. Emission spectra are measured by exciting the QDs with energy higher than their band gap and several parameters are analysed, such as the band-edge peak wavelength and width and the photoluminescence quantum yield (PLQY).

The peak width is characterized in terms of the full width at half maximum (FWHM) that can be measured either in wavelength or energy scale. Due to the inverse relationship between wavelength and energy, evenly spaced data intervals in wavelength are unevenly spaced in energy. Thus, to obtain, a correct calculation of FWHM in energy units (typically meV), the emission spectra measured in a wavelength scale are converted to an energy scale by applying the Jacobian transformation:[29]

$$I(E) = I(\lambda)\frac{\lambda^2}{hc} \quad (1)$$

where $I(E)$ and $I(\lambda)$ are the PL intensity in energy and wavelength units, respectively, $h$ is the Planck's constant and $c$ is the speed of light in vacuum.

The PLQY of the QDs was determined using the standard dye rhodamine 6G at an excitation wavelength of 488 nm. The absorbance at this wavelength was kept below 0.1. The integrated intensities of the emission spectra were corrected for differences in refraction index and concentration, and the PLQY was calculated according to:

$$PLQY = PLQY_{dye}\frac{I_{QD}}{I_{dye}}\frac{A_{dye}}{A_{QD}}\frac{n_{QD}^2}{n_{dye}^2} \quad (2)$$

where $PLQY_{dye}$ is the absolute PLQY reported for Rhodamine 6G (94 % in ethanol),[30] $I$ is the integrated area under the fluorescence spectrum, $A$ is the absorbance at 488 nm, and $n$ is the refractive index of the solvent.

Time-resolved PL spectroscopy enables the study of the decay kinetics and the determination of the radiative lifetime of QDs. The key differences between this technique and steady-state PL spectroscopy is the use of a pulsed source (instead of a continuous light source) and gated detection of the emission, enabling the monitoring of luminescence as a function of time after excitation by the pulse. The radiative lifetime is the average time that the electron-hole pair takes to recombine, after the formation of an exciton. The PL decay curves were fitted with biexponential fits of the form:

$$I(t) = A_1 \exp\left(-\frac{t^2}{\tau_1}\right) + A_2 \exp\left(-\frac{t^2}{\tau_2}\right) \quad (3)$$

The reported average lifetime values are calculated using the fit components as:

$$\tau_{average} = \frac{A_1\tau_1^2 + A_2\tau_2^2}{A_1\tau_1 + A_2\tau_2} \quad (4)$$

Steady-state emission measurements were performed on an Edinburgh Instruments FLS920 fluorescence spectrometer, using a 450W Xe arc lamp as excitation light source. Two different detectors were used; a photomultiplier tube for visible detection (until 850 nm) and a liquid nitrogen cooled Ge-detector for detection above 800 nm. Time-resolved PL measurements used a pulsed LED as excitation source (465 nm) and an ANDOR intensified charge-coupled device.

## 2.3. Elemental analysis

**Inductively coupled plasma optical emission spectrometry**

Inductively coupled plasma optical emission spectrometry (ICP-OES) is used for the elemental quantification of indium. The QD samples are prepared by drying a known volume of a QD suspension in a nitrogen flow and digesting the dried samples in a known volume of nitric acid.

The samples were analysed by means of ICP-OES on a Spectro Arcos instrument, after a 100-fold dilution. Calibration was performed using a set of indium standards with concentrations ranging between 0.1 mg/L and 5 mg/L, and an internal standard was added

to all standards and samples to correct for signal instability and matrix effects. A typical uncertainty on the results is of the order of a few percent.

**Rutherford backscattering spectrometry**

Rutherford backscattering spectrometry (RBS) is used to determine the indium-to-phosphorus ratio $R_{In/P}$. Samples for RBS analysis consisted of films of InP QDs deposited on a MgO substrate by spincoating. $R_{In/P}$ is obtained from the ratio of the backscattered intensity of $He^{2+}$ ions with In and P nuclei after $Z^2$ correction:

$$R_{InP} = \frac{I_{In}}{I_P}\frac{Z_P^2}{Z_{In}^2} \quad (5)$$

where $I_{In}$ and $I_P$ are the integrals of the peaks corresponding to In and P, respectively, and $Z$ is the atomic number.

The measurements were done with an accelerated $He^{2+}$ ion beam and an NEC 5SDH-2 Pelletron tandem accelerator with a semiconductor detector.

**X-ray photoelectron spectroscopy**

X-ray photoelectron spectroscopy (XPS) is a technique that provides qualitative and quantitative elemental analysis, as well as structural information. It measures the binding energy of generated photoelectrons and is used, in this study, to analyse the oxidation state of different elements in a mixture. The samples were prepared by dropcasting and drying a small amount of a solution on a glass plate. The spectra were recorded under ultra-high vacuum conditions using Al $K_\alpha$ primary radiation.

# Chapter 3. Synthesis and optical characterization of InP quantum dots

## 3.1. Introduction

Determining the QD diameter $d_{QD}$ and the concentration of semiconductor material in a QD dispersion is essential in colloidal QD research, from the point of view of characterization, post-synthesis procedures or application of QDs in technological fields.[31] A study of the optical properties of InP QDs is thus essential to (i) establish a sizing curve that relates $d_{QD}$ to the band gap energy $E_g$ and (ii) determine the intrinsic absorption coefficient $\mu_i$ and the molar extinction coefficient $\varepsilon$ that enable the calculation of the concentration of semiconductor material and of QDs in a dispersion, respectively.

In this chapter, a typical synthesis and the structural and optical characterization of InP QDs are described. Then, a sizing curve is established, relating $d_{QD}$ of several batches of InP QDs and the position of the first excitonic absorption peak $\lambda_{1S-1S}$ in the range 520-620 nm. The size dependence of the optical properties of InP at shorter wavelengths is analysed and discussed and $\mu_i$ and $\varepsilon$ are determined. In the end of this chapter, the determined sizing curve and optical parameters are used to study the evolution of the chemical yield and the QD size dispersion during a synthesis.

## 3.2. Synthesis method

The procedure for synthesizing InP QDs is based on a hot-injection method developed by Xie et al.,[18] which consists of mixing an indium precursor and a phosphorus precursor at high temperature in a non-coordinating solvent.

The phosphorus precursor was prepared by mixing 60 µL (0.20 mmol) of tris(trimethylsilyl)phosphine ($P(TMS)_3$), 735 µL (2.20 mmol) of oleylamine (OLA) and 705 µL of 1-octadecene (ODE) in a glovebox under a nitrogen atmosphere. A typical indium precursor was prepared by mixing 117 mg (0.400 mmol) of indium(III) acetate and

388 mg (1.70 mmol) of myristic acid (MA) in 5.00 mL of ODE, and heating for 2 h at 120 ºC under vacuum in a Schlenk line.

Since $P(TMS)_3$ is pyrophoric and the InP QDs are prone to oxidation,[18, 32] the synthesis and work-up were carried out in the glovebox. In a typical synthesis, the indium precursor was loaded into a 50 mL 3-neck flask and the temperature was raised to 188 ºC. The phosphorus precursor was then rapidly injected into the reaction mixture and the temperature was reduced and maintained at 178 ºC for the growth of the nanocrystals. The reaction was stopped after 1h by temperature quenching with 3 mL of ODE. During the reaction, aliquots were taken at different reaction times and collected in toluene to follow the growth of the QDs by absorption spectroscopy (Figure 5).

The final product of the synthesis was diluted in toluene and purified by subsequent cycles of precipitation with a non-solvent mixture, centrifugation for 5 min at 3500 rpm and redispersion in toluene. During the first two purification cycles, a mixture of isopropanol and methanol was used to precipitate the nanoparticles and, in the following cycles, methanol was replaced by acetonitrile, to avoid stripping the ligands from the QD surface by methanol.[33] After 6 to 8 purification cycles, the InP QDs were dispersed in a small amount of toluene and stored in the glovebox.

Xie et al.[18] found that the most convenient method to tune the QD size was by varying the concentration of MA in the reaction mixture, with an increasing concentration of this fatty acid yielding larger QDs. Therefore, to obtain QDs with different sizes, a variable amount of MA (from 1.55 to 1.90 mmol) was added to prepare the indium precursor used in each synthesis.

## 3.3. Characterization of the nanocrystals

This section describes the characterization of a sample of InP QDs prepared using the typical synthesis procedure described above. As mentioned, collecting aliquots during the synthesis enables the monitoring of the growth of the QDs. Figure 5 represents the temporal evolution of the absorption spectra of several aliquots collected at different times. In an early stage of the synthesis, only 30 s after the injection of the phosphorus precursor, the absorption spectrum presented a maximum of $\lambda_{1S-1S}$ at 451 nm. During the reaction

this peak was red shifted and after 60 min it was located at 572 nm, confirming that the QD size had increased.

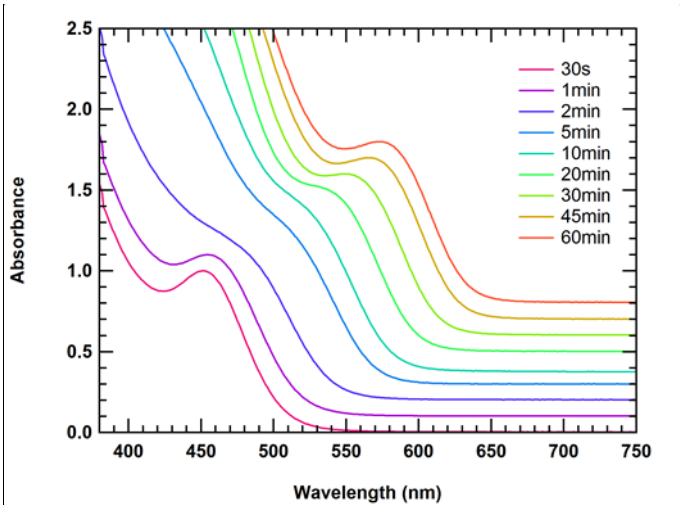


Figure 5. Absorption spectra of aliquots taken at different times during the synthesis of InP QDs. The spectra were normalised at $\lambda_{1S-1S}$ and shifted vertically for clarity.

Regardless the evolution of the first excitonic absorption peak, which is not well--defined from 2 min to 20 min, in the end of the synthesis this peak is again relatively sharp and distinct, suggesting low size dispersion. This is a good indication that this synthesis method enables the fabrication of fairly monodisperse QDs, in contrast with other previously reported methods,[6, 16, 19] where additional post-synthetic size-selective precipitation was required to narrow the size distribution.

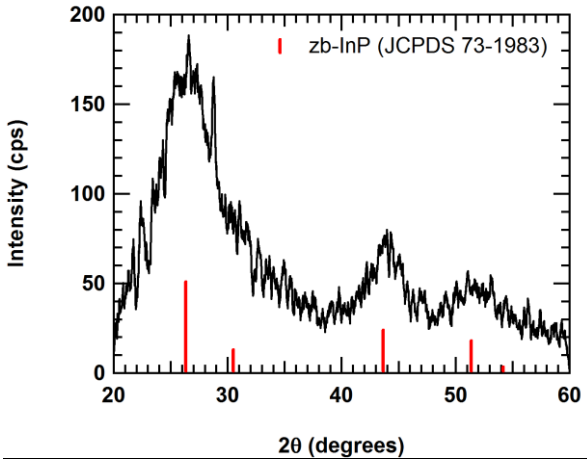


Figure 6. X-ray diffractogram of InP QDs. The vertical red lines indicate the characteristic peak positions of bulk zinc blende InP.

The structural characterization of the synthesized InP QDs was done with XRD and TEM. Figure 6 presents the X-ray diffractogram of the nanoparticles, revealing a crystal structure that matches the reflections of bulk InP with a cubic zinc blende structure. The diffraction peaks are broad, since, according to Scherrer equation, the peak width is inversely proportional to the average size of the monocrystalline QDs.[27] In Figure 7, two images obtained by TEM are exhibited. These demonstrate that fairly isotropic and uniform nanoparticles were formed, with low size polydispersity. From the surface area of the imaged nanoparticles, and assuming they are spherical, the determined average QD diameter $d_{QD}$ was 3.25±0.32 nm, for a total of 140 measured QDs.

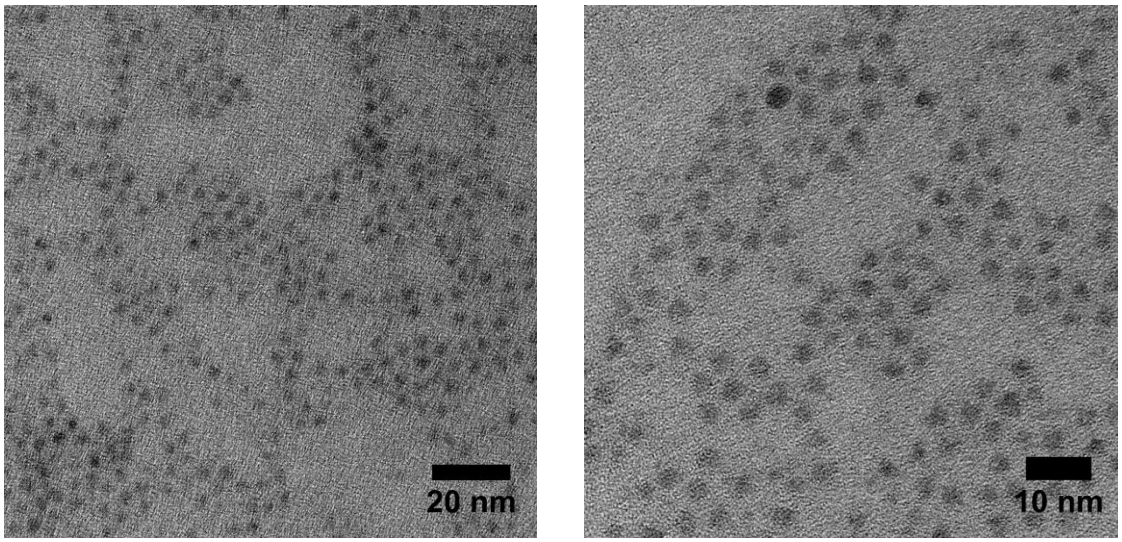


Figure 7. TEM images of the synthesized InP QDs.

To quantitatively analyse the amount of indium in the QDs, it is necessary that no other indium-containing species (such as indium myristate) are present in the QD dispersion, in which case the amount of InP is overestimated. The purity of the dispersion was assessed by suspending the QDs in toluene-d8 and obtaining a $^{1}$H NMR spectrum.[34] This technique also enables a quantitative analysis of the ligands that are bound to the QD surface.

Figure 8 shows that, apart from the resonances from toluene and impurities, no sharp signals arising from free species as indium myristate or OLA (which could possibly complex with indium) were present in the QD dispersion. The broad resonances correspond to bound ligands capping the QD surface, mainly deprotonated MA (Figure

8b), which is a negatively charged X-type ligand that binds covalently to the QD surface.[35] Broad proton resonances at 5.60 ppm and 2.65 ppm were attributed to bound OLA ligands (see spectrum of unbound OLA in Figure 8c), meaning that OLA was also part of the ligand shell. This is, in fact, a neutral L-type ligand, which binds datively (therefore more loosely than X-type ligands) to the QD surface.[35]

The broad resonances at 5.60 ppm (attributed to the two olefinic protons from OLA) and 1.05 ppm (the three methyl protons from both MA and OLA) can provide an estimation of the proportion of MA and OLA capping the QD surface. The ratio of their integrals is 2 to 23.1, which means that for each molecule of bound OLA there are 6.7 molecules of bound MA.

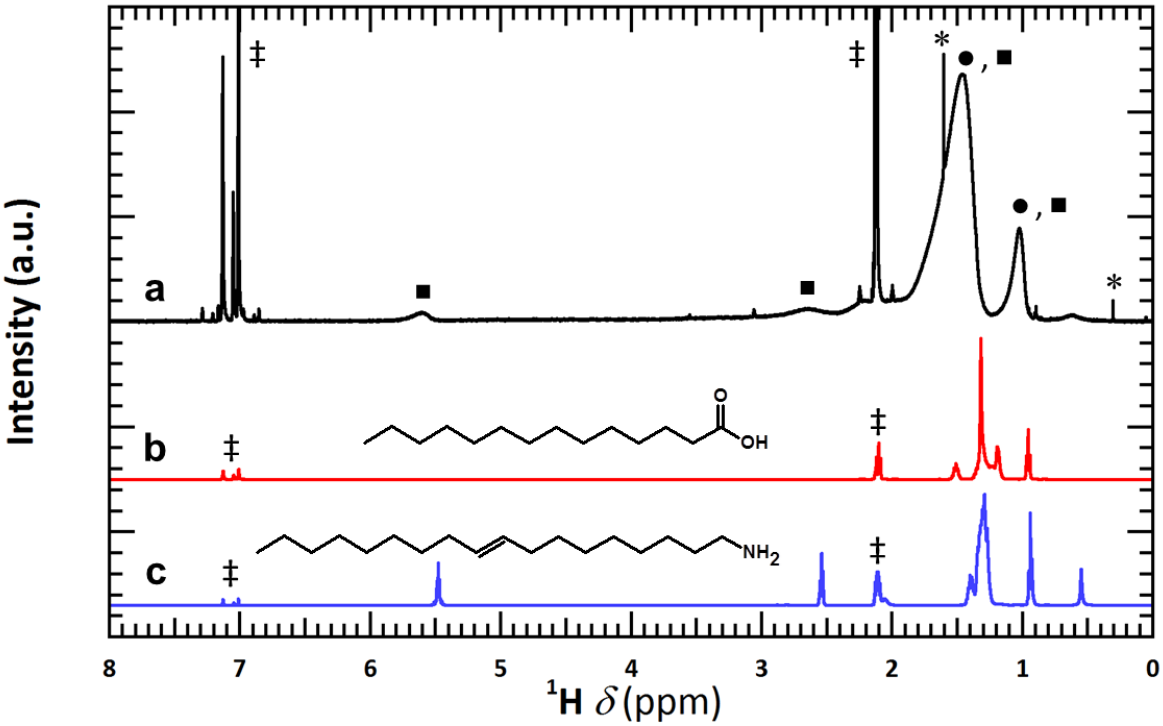


Figure 8. (a) $^{1}$H NMR spectrum of a QD dispersion of InP in toluene d-8 (● and ■ represent the resonances assigned to MA and OLA, respectively). Structure and $^{1}$H NMR spectrum of (b) MA and (c) OLA in toluene-d8. ‡ indicates resonances from solvent and * from impurities.

## 3.4. Sizing curve

Due to quantum confinement effects, knowing the average size of a batch of QDs is utterly important to understand and predict many of their size-dependent properties. The diameter of spherical nanoparticles can be obtained directly by TEM imaging and determining the average QD diameter, but this is a time-consuming operation and requires a lot of tedious data processing. In the case of small InP QDs, a good contrast between particles and background is difficult to obtain,[6, 20, 27] making this data processing even more challenging. A more straightforward method to determine $d_{QD}$ consists of relating it to the wavelength of the first excitonic absorption peak maximum $\lambda_{1S-1S}$, as this depends on the QD size.

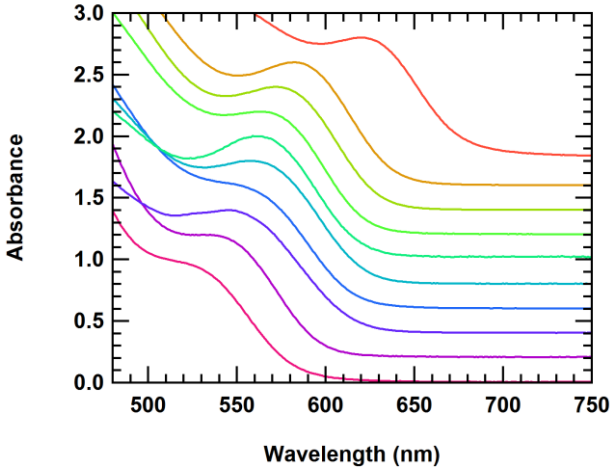


Figure 9. Absorption spectra of 10 batches of differently sized InP QDs from different syntheses, used to construct the sizing curve. The spectra were normalised at $\lambda_{1S-1S}$ and shifted vertically for clarity.

In order to obtain a sizing curve that relates this absorption peak to $d_{QD}$, 10 batches of InP QDs were synthesized and purified, with $\lambda_{1S-1S}$ ranging from 521 nm to 619 nm (Figure 9). Several TEM images of each QD dispersion were then obtained, to have a representative sample, and the average diameter was determined (see section 2.1). Table 1 summarises the combined results from absorption spectroscopy and TEM that enabled the construction of the sizing curve.

Table 1. Wavelength of the first excitonic peak maximum and HWHM (from absorption spectroscopy) and mean diameter, standard deviation and number of measured QDs (from TEM).

| $\lambda_{1S-1S}$ (nm) | HWHM (nm) | $d_{QD}$ (nm) | $\sigma_d$ (nm) | Measured QDs |
|---|---|---|---|---|
| 521 | 38 | 2.96 | 0.41 | 126 |
| 537 | 37 | 2.88 | 0.29 | 135 |
| 545 | 43 | 3.02 | 0.39 | 185 |
| 551 | 41 | 3.18 | 0.38 | 214 |
| 558 | 40 | 3.07 | 0.29 | 151 |
| 561 | 36 | 3.06 | 0.38 | 266 |
| 563 | 38 | 3.10 | 0.39 | 187 |
| 572 | 36 | 3.25 | 0.32 | 141 |
| 581 | 36 | 3.25 | 0.33 | 180 |
| 619 | 37 | 3.72 | 0.40 | 80 |

Figure 10 displays the different data points obtained for the band gap energy $E_g$ (in eV) as a function of $d_{QD}$ (in nm). The results from the 10 batches of QDs were used together with those obtained by Lambert[6] to construct the sizing curve and very good agreement between both sets of data was found. The red line in Figure 10 represents the best fit to the experimental data, which was given by the following empirical formula:

$$E_g = 1.35 + \frac{1}{(0.119 \pm 0.003) d_{QD}^2} \quad (6)$$

This sizing curve fits well the data points and is in agreement with the sizing curves determined by other authors[19-20, 36] and can thus be used to easily and reliably estimate $d_{QD}$ from the absorption spectrum of a dispersion of QDs, in the range of 1.7 eV to 2.5 eV. Band gap energies outside of this interval will be calculated based on an extrapolation from the fit, with additional error on the estimation.

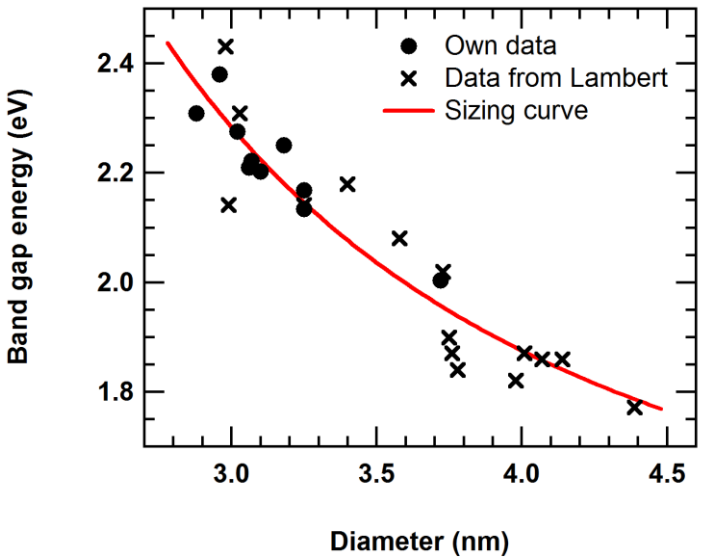


Figure 10. Plot of the energy of the first excitonic peak versus the nanoparticle diameter of synthesized InP QDs (circles) and obtained by Lambert (crosses). The red line represents the best fit of the experimental data, according to equation ( 6 ).

## 3.5. Intrinsic absorption coefficient

The intrinsic absorption coefficient $\mu_i$ can be used to determine the concentration of InP in a colloidal dispersion of QDs,[37] as it relates the absorbance $A$ to the QD volume fraction $f$:

$$\mu_i = \frac{A \ln 10}{f L} \quad (7)$$

where $L$ is the path length.

The volume fraction, which is the volume occupied by the QDs per unit of sample volume, describes the composition of the colloidal dispersion and is given by:[31]

$$f = \frac{V_m n_{InP}}{V_{total}} = V_m \frac{C_{In}}{2}\left(1 + \frac{1}{R_{In/P}}\right) \quad (8)$$

where $V_m$ is the molar volume of InP (0.0303 L/mol), $n_{InP}$ is the amount of material, $C_{In}$ is the molar concentration of indium and $R_{In/P}$ is the indium-to-phosphorus ratio.

$\mu_i$ can thus be calculated by combining elemental analysis (to determine $f$) and absorption spectroscopy (to determine $A$). In this study, $C_{In}$ of six batches of differently

sized InP QDs was quantified by ICP-OES. Phosphorus analysis by this technique is unreliable as the nanocrystals are dissolved in a solution of nitric acid and therefore phosphine ($PH_3$), which is a gas at room temperature, can be formed during this process. Hence, RBS was used to determine $R_{In/P}$ of one of the samples and the obtained value was employed as the ratio for the remaining samples. Table 2 presents the measured values of $C_{In}$ and $R_{In/P}$, as well as the calculated $f$ values, for the six samples.

Table 2. Volume fraction of six samples of InP QDs.

| $d_{QD}$ (nm) | $C_{In}$ (mmol/L) | $R_{In/P}$ | $f$ ($10^{-4}$) |
|---|---|---|---|
| 3.72 | 6.79 | - | 1.85 |
| 3.25 | 22.0 | - | 6.01 |
| 3.25 | 29.7 | 1.25 | 8.10 |
| 3.02 | 19.3 | - | 5.27 |
| 2.88 | 27.6 | - | 7.53 |
| 2.48* | 30.8 | - | 8.39 |

* Diameter estimated from the sizing curve

The absorption spectra of these samples were combined with the $f$ values to calculate $\mu_i$ according to equation ( 7 ), and the $\mu_i$ spectra are shown in Figure 11a. Previous studies on the optical properties of other semiconductor nanocrystalline materials[31, 34, 38-39] demonstrated that $\mu_i$ spectra of differently sized QDs coincide at short wavelengths. This trend was observed for InP QDs at wavelengths below 440 nm, especially around 335 nm and 410 nm (Figure 11b and c), where the relative standard deviation from the average value $\bar{\mu}_i$ was smaller (Figure 11d), suggesting that the quantum confinement effects were minimal at these wavelengths.

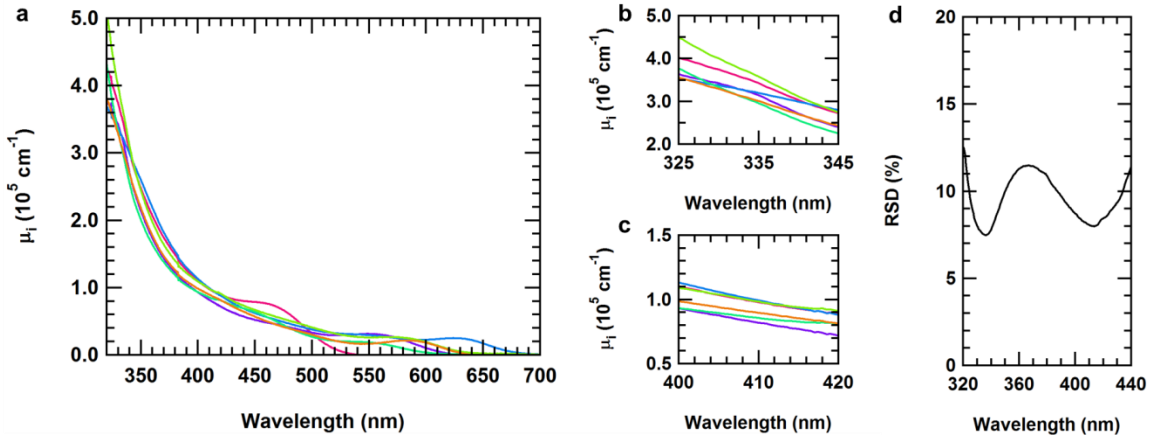


Figure 11. (a) $\mu_i$ spectra of six differently sized samples of InP QDs in chloroform. (b, c) Zoom of (a) in the range 325 nm to 345 nm and 400 nm to 420 nm, respectively. (d) Relative standard deviation on $\mu_i$ as a function of wavelength calculated using the six spectra shown in (a).

Table 3 displays $\bar{\mu}_i$ at 335 nm and 410 nm, as well as the relative standard deviation of the experimental determination. As mentioned, the best overlap for $\mu_i$ of the analysed samples was found around these two wavelengths, and so these should be preferably used to calculate the concentration of InP in a sample. Nevertheless, QDs with a diameter below the range of the ones analysed (smaller than around 2.5 nm), could possibly show quantum confinement effects at 410 nm, since their first excitonic transition would have a maximum close to this wavelength. In this case, $\mu_i$ at 410 nm would not be suitable to calculate the concentration of InP and the value at 335 nm should be used instead.

Table 3. $\bar{\mu}_i$ for InP in chloroform at 335 nm and 410 nm.

| $\lambda$ (nm) | $\bar{\mu}_i$ ($10^5$ cm$^{-1}$) | RSD$_{\bar{\mu}_i}$ (%) |
|---|---|---|
| 335 | 3.22 | 7.56 |
| 410 | 0.920 | 8.08 |

Due to the lack of quantum confinement effects in the higher energy region of the spectra, a good match is usually obtained between $\mu_i$ of QDs and of the bulk material.[37-38] The theoretical $\mu_{i,th}$ can be calculated by using the optical constants for bulk InP:[37, 40-41]

$$\mu_{i,th} = \frac{4\,\pi\,n\,k\,|f_{LF}|^2}{n_s\,\lambda} \qquad (9)$$

where $n$ and $k$ are the real and imaginary parts of the refractive index of bulk InP, $n_s$ is the refractive index of the solvent and $f_{LF}$ is the local field factor, which represents the ratio between the electric field inside and outside of the QD and is given by:

$$|f_{LF}|^2 = \frac{9{n_s}^4}{\left(n^2 - k^2 + 2{n_s}^2\right)^2 + 4(nk)^2} \quad (10)$$

The refractive index of the ligand shell is not taken into account in the calculation of $\mu_{i,th}$ from equation ( 9 ). Therefore, the refractive indices of the solvent and of the ligand shell should ideally match or, at the very least, be as similar as possible for this equation to be applicable.[38] In the case of the studied InP QDs, the ligand is myristic acid, whose refractive index ($n_D^{20}$=1.431) almost matches that of chloroform ($n_D^{20}$=1.446), and so this solvent was used both in the absorbance measurements for the determination of $\mu_i$ and in the calculation of $\mu_{i,th}$, for a more accurate comparison.

Figure 12a represents the bulk $\mu_{i,th}$ spectrum of InP in chloroform, calculated from equation ( 9 ). A particular absorption feature is clearly seen in the region 280-400 nm, which is distinct from what is observed in the spectra of the QDs. A similar characteristic was reported by Kamal et al.[31] in the bulk $\mu_{i,th}$ spectrum of CdTe (see inset of Figure 12a) and it was attributed to the transition connecting the initial and final states along the Λ direction in the Brillouin zone.[31, 42] This is in agreement with the absence of this feature in the spectra of the QDs, as such transitions would be less pronounced and shifted to higher energy values and thus would not be seen above 320 nm.

The mismatch between bulk and nanocrystalline InP means that quantum confinement effects in the absorption spectra are still present at wavelengths shorter than 400 nm. Although they are not detectable in the $\mu_i$ spectra of the studied QDs, this may not be the case for large QDs with diameters closer to the exciton Bohr diameter. The $\mu_i$ spectrum of such nanocrystals would likely show a similar feature to the bulk $\mu_{i,th}$, as it was observed for large CdTe QDs (red lines in the inset of Figure 12a).[31] In this case, the absorption at wavelengths below 400 nm cannot be used to determine the concentration of InP since, as it is suggested, considerable size effects on $\mu_i$ would be present, and the $\mu_i$ determined at 410 nm may provide a more accurate estimation of the concentration.

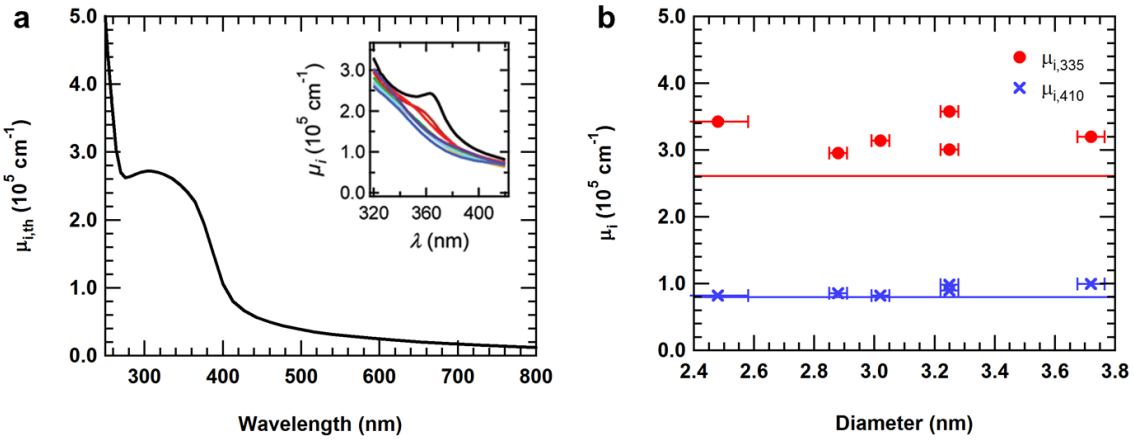


Figure 12. (a) $\mu_{i,th}$ calculated for bulk InP in chloroform. (Inset) $\mu_i$ spectra of CdTe QDs of different sizes and $\mu_{i,th}$ (black line) calculated for bulk CdTe. Reproduced from Kamal et al. (2012).[31] (b) $\mu_i$ of six samples at 335 nm (red circles) and 410 nm (blue crosses) as a function of $d_{QD}$. The horizontal lines represent $\mu_{i,th}$ at these wavelengths. The error bars of the experimental points represent the standard error of the mean.

As already mentioned, $\mu_i$ values were in good agreement, especially at 335 nm and 410 nm, in the range of diameters of the analysed samples (around 2.5-3.7 nm). Figure 12b shows $\mu_{i,335}$ and $\mu_{i,410}$ as a function of $d_{QD}$, confirming that both values are size--independent. The horizontal lines correspond to $\mu_{i,th}$ at each wavelength and the average experimental values $\bar{\mu}_{i,335}$ and $\bar{\mu}_{i,410}$ are higher than those by 23 % and 14 %, respectively. These differences are not surprising, due to the size effects discussed in this section.

## 3.6. Molar extinction coefficient

The molar extinction coefficient $\varepsilon$ for QDs with a given diameter $d_{QD}$ can be calculated from $\mu_i$ as:[37]

$$\varepsilon = \frac{\pi d_{QD}^3 N_A}{6 \ln 10} \mu_i \qquad (11)$$

where $N_A$ is the Avogadro's number.

Figure 13 presents $\varepsilon_{335}$ and $\varepsilon_{410}$ for the six InP QD samples as a function of $d_{QD}$. The data were fitted to a $d_{QD}^3$ power law (full lines in the figure) and the obtained equations for $\varepsilon_\lambda$ (in $cm^{-1}$ $mol^{-1}$ L) were ($d_{QD}$ is given in nm):

$$\varepsilon_{335} = (4.40 \pm 0.19) \times 10^4 \, d_{QD}^3 \qquad (12)$$

$$\varepsilon_{410} = (1.29 \pm 0.06) \times 10^4 \, d_{QD}^3 \qquad (13)$$

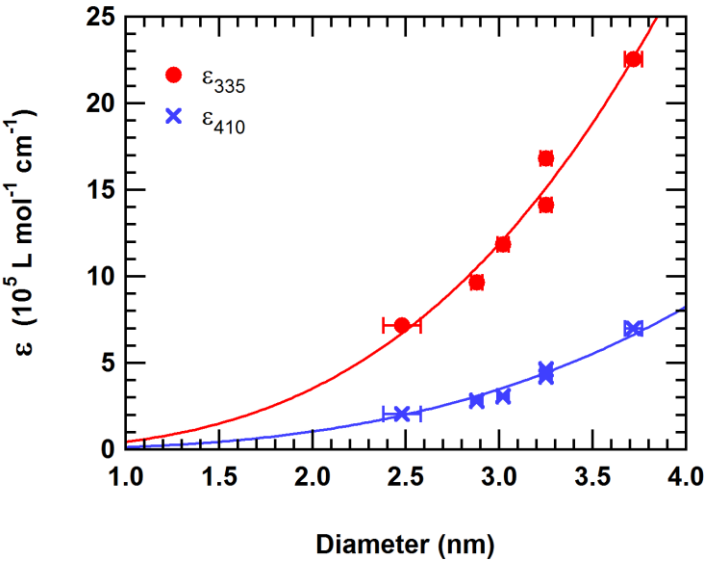


Figure 13. Molar extinction coefficient $\varepsilon$ of 6 samples at 335 nm (red circles) and 410 nm (blue crosses) as a function of $d_{QD}$. The trend lines show the best fit of the data to a $d_{QD}^3$ power law. The error bars of the experimental points represent the standard error of the mean.

It can be seen in Figure 13 that, for both wavelengths, $\varepsilon$ scaled well with the QD volume, confirming that the $\bar{\mu}_i$ values found in the previous section are size-independent. A similar trend was found for InP QDs with different ligands and solvents, namely, InP QDs capped with tri-n-octylphosphine oxide and dispersed in n-hexane[26] and InP QDs capped with and dispersed in pyridine.[6] However, different values were obtained for the coefficient in the $d_{QD}^3$ fit (respectively, $3.86\times10^4$ and $3.45\times10^4$ $cm^{-1}$ $mol^{-1}$ L $nm^{-3}$), since the absorbance was measured at 350 nm and different solvents and capping ligands were used.

Equations ( 12 ) and ( 13 ) are very useful as, together with the sizing curve given in equation ( 6 ), they enable the direct determination of the concentration of InP QDs from the absorption spectrum, using the Lambert-Beer law.

## 3.7. Using the sizing curve and the optical parameters

To demonstrate the practical interest of the sizing curve and the optical parameters determined in the previous sections, these were utilised to study the evolution of different quantities in a synthesis of InP QDs, namely the chemical yield, the diameter and the size dispersion. For this, quantitative aliquots were collected during a synthesis in 3.00 mL of chloroform and their mass was measured in order to calculate the weight fraction of each aliquot related to the total mass of the reaction mixture. This synthesis was performed according to the procedure described in the next chapter (see section 4.2), where 0.90 mmol of indium was used as the limiting reagent.

Using equations ( 7 ) and ( 8 ), the amount of indium in the QD dispersion is obtained from the indium-to-phosphorus ratio, and the intrinsic absorption coefficient and the absorbance at short wavelengths. Thus the chemical yield $CY_{In}$, related to the amount of indium $n_{In,init}$ used, can be calculated as:

$$CY_{In} = \frac{1}{n_{In,init}} \frac{m_{total}}{m_{aliq}} \frac{V_{aliq}}{V_m} \frac{2\,R_{In/P}}{1 + R_{In/P}} \frac{A\,ln10}{L\,\mu_i} \qquad (14)$$

where $m_{total}$ and $m_{aliq}$ are the mass of the synthesis reagents and of the aliquot, respectively, and $V_{aliq}$ is the volume of chloroform in which each aliquot was collected.

The size dispersion $\sigma_d$ was estimated from the half width at half maximum (HWHM) of the first excitonic peak according to (the derivative $\partial(d_{QD})/\partial\lambda$ is calculated using the sizing curve):[43]

$$\sigma_d = \frac{1}{d_{QD}} \frac{HWHM}{\sqrt{2\ln 2}} \left| \frac{\partial(d_{QD})}{\partial\lambda} \right| \qquad (15)$$

Table 4 indicates the time at which each aliquot was collected, as well as the respective weight fraction, the absorbance at 335 nm and 410 nm and the wavelength and HWHM of the first excitonic peak.

Table 4. Weight fraction, absorbance at 335 nm and 410 nm, and wavelength and HWHM of the first excitonic peak of aliquots collected throughout the synthesis

| Time (min) | Weight fraction (%) | $A_{335}$ (nm) | $A_{410}$ (nm) | $\lambda_{1S-1S}$ (nm) | HWHM (nm) |
|---|---|---|---|---|---|
| 5 | 1.190 | 0.9646 | 0.3665 | 527 | 47 |
| 10 | 0.576 | 0.8093 | 0.2703 | 542 | 35 |
| 20 | 1.033 | 2.3886 | 0.8205 | 558 | 34 |
| 30 | 0.879 | 2.4494 | 0.8424 | 567 | 33 |
| 40 | 0.931 | 2.8215 | 0.9788 | 572 | 34 |
| 50 | 0.896 | 2.9374 | 1.0216 | 575 | 35 |
| 60 | 0.940 | 3.2531 | 1.1697 | 577 | 38 |

Apart from the first two aliquots, the absorbance values measured at 335 nm were higher than 2, i.e., more than 99 % of the incident radiation was absorbed by the sample at this wavelength, which can lead to deviations from linearity of the Lambert-Beer law. Therefore, to calculate the chemical yield, only the absorbance values at 410 nm were considered. Figure 14a presents a plot of the chemical yield over time, which increased gradually, during the whole synthesis, reaching 38.1 % after 60 min.

Figure 14b displays $d_{QD}$, obtained from the sizing curve, and $\sigma_d$, obtained from equation ( 15 ), for the different aliquots. The size dispersion was focused during the first 30 min and increased thereafter, being 7.52 % at the end of the synthesis.

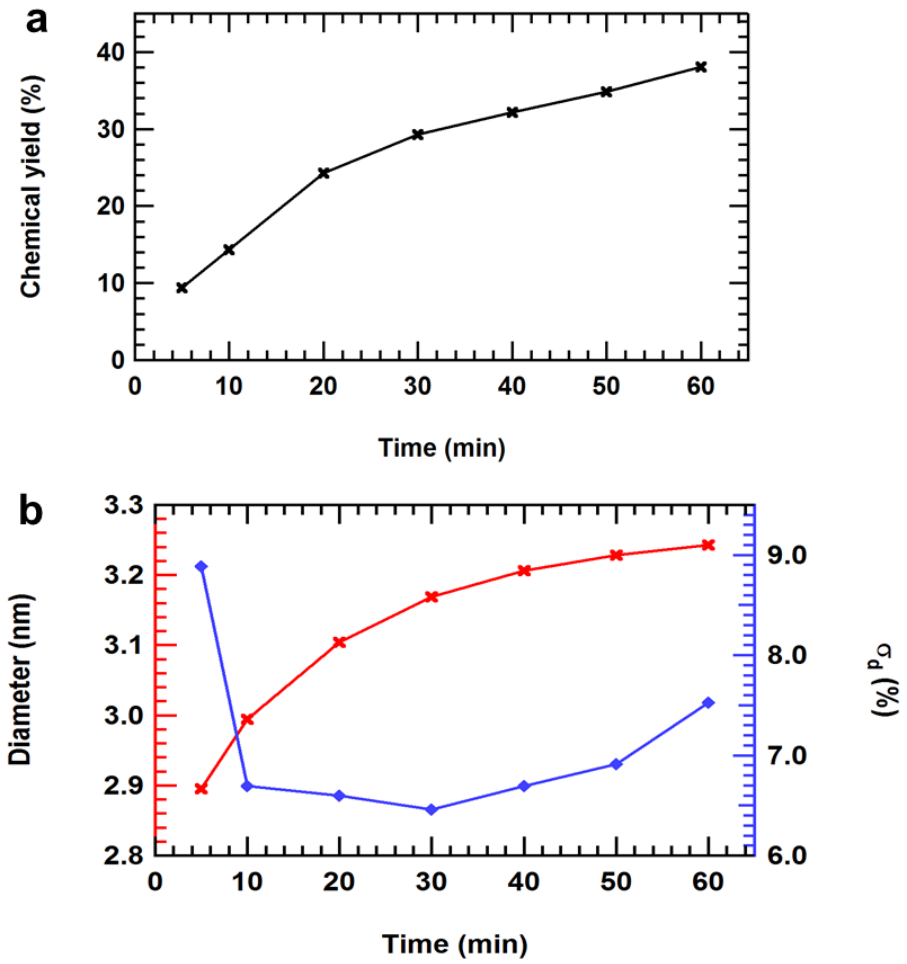


Figure 14. (a) Evolution of the chemical yield with time (b) Evolution of $d_{QD}$ (red) and $\sigma_d$ (blue) with time.

# Chapter 4. New route for the one-pot synthesis of InP/CdS quantum dots

## 4.1. Introduction

The synthesis method reported in the previous chapter makes use of $P(TMS)_3$ as the phosphorus precursor. Since it was firstly reported, most of the InP QD syntheses rely on this method with some modifications, as it yields relatively monodisperse QDs having distinct absorption features.[21-25, 27, 36] Nevertheless, the use of $P(TMS)_3$ is quite problematic as this is a highly expensive and extremely toxic reagent, being unsuitable for scaling up of the production of InP QDs. Very recently, a new route for the colloidal synthesis of high--quality InP/ZnS QDs was developed by Song et al.,[44] using tris(dimethylamino)phosphine, $P(DMA)_3$, which is a much cheaper and more sustainable phosphorus precursor.

In this chapter, we report the applicability of this new strategy to the one-pot synthesis of InP/CdS QDs. Initially, a typical synthesis of InP/CdS is described and the resulting QDs are characterized and compared with InP/ZnS QDs synthesized in similar conditions. Then, we focus on the PL properties of these QDs, tuning their emission from the visible to the NIR region by changing the size of the InP cores. Finally, time-resolved PL measurements are performed to estimate the radiative lifetime of InP/ZnS and InP/CdS QDs.

## 4.2. Synthesis method

Song et al.[44] established a new one-pot hot-injection synthesis for the formation of InP/ZnS QDs, making use of $P(DMA)_3$ instead of $P(TMS)_3$ and replacing ODE, used as non-coordinating solvent in the previously described synthesis, by OLA, a relatively weak coordinating solvent. Briefly, this method consists of mixing indium(III) chloride and zinc chloride with OLA, heat to high temperature and inject $P(DMA)_3$, leading to the formation of InP core QDs. After some time, 1-dodecanethiol (DDT) was added, enabling the epitaxial shell growth of ZnS.

To investigate the formation of InP/CdS QDs using this procedure, zinc chloride was replaced by cadmium chloride. In a typical synthesis, 199 mg (0.90 mmol) of indium(III) chloride and 181 mg (0.90 mmol) of cadmium chloride monohydrate were mixed with 5.00 mL of OLA in a 25 mL 3-neck flask. The mixture was magnetically stirred, degassed at 100 ºC for 30 min and subsequently heated to 180 ºC under nitrogen flow. 0.25 mL (1.4 mmol) of $P(DMA)_3$ were then rapidly injected, initiating the growth of the core nanocrystals. After 10 min, 0.50 mL of a 2 M solution of sulfur in tri-n-octyl-phosphine were injected dropwise and the temperature was kept at 180 ºC for 1h, being then increased to 220 ºC and the mixture was maintained at that temperature for 2 h more. Tri-n-octylphosphine sulphide (TOPS) was used as the sulfur precursor during the shell growth since prior experiments made by our group showed that a lower amount of this precursor (compared to DDT, which was added in excess) enabled the synthesis of bigger shells, without the blue shift observed when DDT was used.[44]

Finally, the reaction was quenched with a water bath and 1 mL of oleic acid was added to the mixture. The final product of the synthesis was diluted in chloroform and purified twice by successive cycles of precipitation with ethanol, centrifugation for 4 min at 4000 rpm and redispersion in chloroform.

## 4.3. Characterization of the nanocrystals

In this section, a sample of InP/CdS QDs synthesized according to the procedure described above is characterized. One other sample of InP/ZnS QDs was synthesized following the same procedure (replacing cadmium chloride by zinc chloride) and a comparison is established between the two.

Figure 15 displays the absorption spectra of several aliquots collected in toluene at different times during the syntheses of InP/ZnS and InP/CdS to follow the growth of the QDs. In the case of InP/ZnS, a red shift of $\lambda_{1S-1S}$ was observed during the core growth from 445 nm (at 30 s) to 560 nm after 10 min, corresponding to a QD diameter of 3.12 nm, according to the sizing curve established in the previous chapter. After TOPS was injected, $\lambda_{1S-1S}$ continued shifting until 575 nm (1 h later), reaching 590 nm after 2 h at 220 ºC. This shift of the first excitonic peak suggested that a complete growth of the InP cores had not occurred and continued even after the injection of TOPS. A small red shift (5-10 nm)

during the shell growth is characteristic from type-I core-shell structures as a result of a partial leakage of the exciton into the shell material,[15] but the pronounced shift that was observed is more likely due to the increase of the size of core InP than to the epitaxial growth of ZnS.

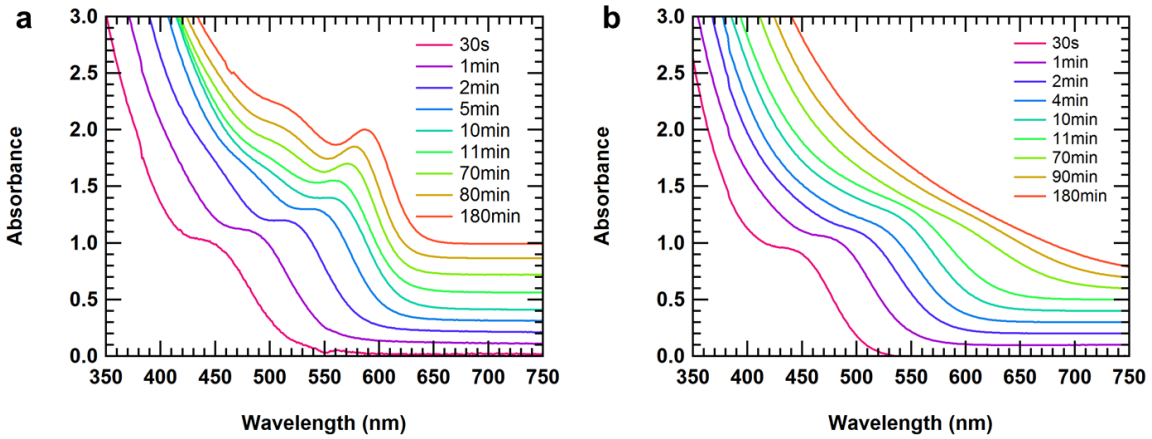


Figure 15. Absorption spectra of aliquots taken at different times during the syntheses of (a) InP/ZnS and (b) InP/CdS QDs. The spectra were normalised and shifted vertically for clarity.

During the synthesis of core InP QDs in the presence of cadmium chloride (Figure 15b), $\lambda_{1S-1S}$ was red shifted from 445 nm at 30 s (the same value found for InP/ZnS QDs) to 532 nm after 10 min, resulting in QDs with a diameter of 2.9 nm. This smaller shift, compared to InP/ZnS, may indicate that the InP QD growth is slowed down by the presence of $Cd^{2+}$ ions on their surface. This was also observed in the original study, where the effect of $Zn^{2+}$ ions was analysed by comparing the evolution of $\lambda_{1S-1S}$ with and without zinc chloride in the mixture. When zinc chloride was added, a narrower excitonic peak was observed at shorter wavelengths, which was attributed to the stabilisation of the QD surface and the reduction of the critical nuclei size, resulting in smaller QDs.[22, 44] A broader size distribution was observed for InP core QDs synthesized in the presence of cadmium chloride, suggesting that the stabilisation of the QD surface is more effective with $Zn^{2+}$ than with $Cd^{2+}$.

In the synthesis of InP/CdS QDs, the first excitonic absorption peak became less distinct during the shell growth until it vanished completely. This was consistent with the formation of a type-II core-shell structure, as there is only a small overlap of the hole and the electron wavefunctions due to the spatial separation of the two charge carriers.[17, 45-46]

During both InP/ZnS and InP/CdS syntheses, the emission of visible light was observed under UV excitation, even from early stages of the core growth, confirming the passivation of the QD surface by $Zn^{2+}$ and $Cd^{2+}$, respectively. This leads to a reduction of the number of surface dangling bonds that act as trap states, enhancing band-edge emission.[15]

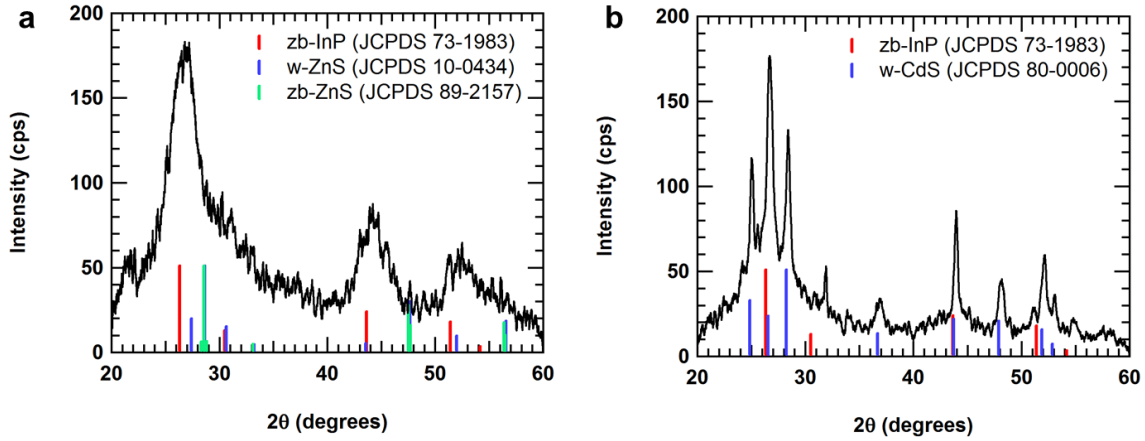


Figure 16. X-ray diffractograms of (a) InP/ZnS and (b) InP/CdS QDs. The characteristic reflections of each crystal structure are displayed in the vertical lines.

Both core-shell QDs were structurally characterized by XRD and the respective X-ray diffractograms are shown in Figure 16. The first is dominated by the characteristic peaks of a zinc blende structure of InP, possibly suggesting that a thin shell was grown. The crystal structure of the shell material is not so evident, partly because of the small amount of ZnS material and also because both zinc blende and wurtzite peaks of bulk ZnS overlap with each other or with zinc blende InP peaks. Although it would be more reasonable that the more stable zinc blende crystal structure was formed, following the epitaxial growth of ZnS on the zinc blende cores, a InP/ZnS heterostructure with a zinc blende core and wurtzite shell is not unsuitable for two main reasons. First, there is a small mismatch between the lattice parameters of the two ZnS crystal structures compared to zinc blende InP, that may not affect significantly the epitaxial growth of the shell material. Moreover, the energy difference between the two crystal structures is small and ZnS exhibits strong polytypism in the bulk.[47] This has also been observed in core-shell nanostructures, where InP/ZnS QDs with zinc blende core and wurtzite shell have already been reported.[16]

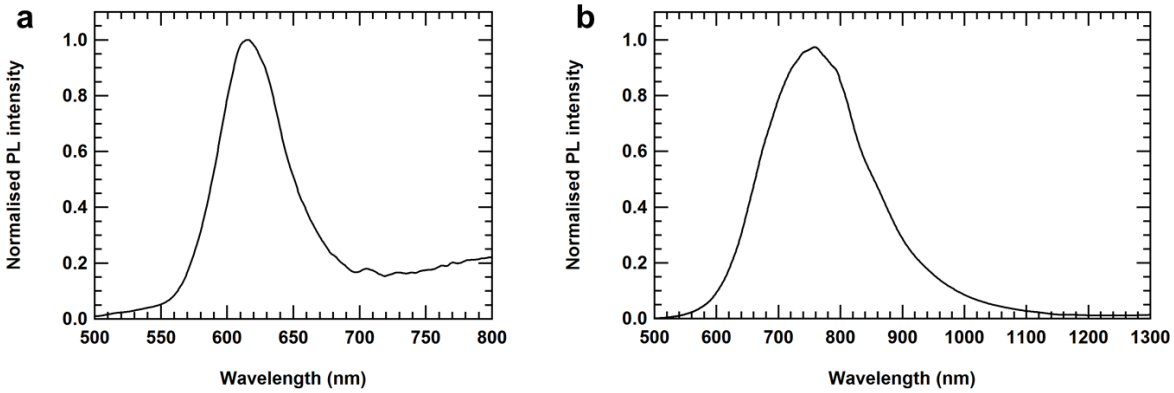


Figure 17. Normalised PL spectra of (a) InP/ZnS and (b) InP/CdS QDs, excited at 488 nm.

The analysis of the diffractogram of InP/CdS QDs is clearer as the characteristic reflections of both zinc blende InP and wurtzite CdS are well defined. In this case, it would again be expected that the core and the shell materials crystallize in the same structure, to minimise the formation of strain-induced defect states.[15] Nevertheless, as with the InP/ZnS core-shell structure, the mismatch between the lattice parameters of zinc blende InP ($a$=5.869Å) and the wurtzite CdS ($\sqrt{2}a_w$=5.850Å) is only 0.3 % and is even smaller than it would be with zinc blende CdS ($a$=5.832Å).[48] The diffraction peaks attributed to CdS are considerably narrow, which may indicate the formation of a thick shell or, on the other hand, the occurrence of secondary nucleation of larger CdS QDs.

The PL spectra of the two core-shell heterostructures are presented in Figure 17. The synthesized InP/ZnS QDs showed weak band-edge emission at 617 nm with a FWHM of 58 nm (218 meV). The PLQY was calculated to be only 7 %. This low value was not surprising since strong trap emission at lower energy was clearly observed, meaning that an inefficient passivation of the core QD surface was obtained and the consequent presence of trap states inhibited the PLQY by acting as fast non-radiative de-excitation channels for exciton recombination.[15]

The InP/CdS QDs exhibited a stronger band-edge emission at 755 nm, with a large FWHM of 190 nm (460 meV) and PLQY around 37 %. In this sample, no trap emission was observed, denoting a good surface passivation by the CdS shell, with a low amount of interfacial defects. This spectrum was obtained by matching the partial spectra acquired with a visible detector and a NIR detector, measuring the PL in the range 500-800 nm and 700-1300 nm, respectively, and thus there might be a larger error in the determination of the PLQY for this sample.

## 4.4. Tuning the band-edge emission of InP/CdS

In this section, the emission wavelength of InP/CdS QDs was tuned by synthesizing QDs with different core diameters. This was achieved by varying the reaction temperature during the core growth, as increasing temperatures resulted in larger InP core diameters, due to a higher rate of formation of InP nuclei.[24]

Four syntheses of InP/CdS QDs were performed, with core growth temperatures ranging from 120 ºC to 220 ºC. The time of the InP core synthesis could be greatly reduced by increasing the temperature: while the smaller core QDs were synthesized at 120 ºC during 60 min, the larger ones were grown at 220 ºC for only 3 min. Figure 18 displays the absorption spectra of the core QDs of the four syntheses, which were obtained just before the injection of TOPS and, thus, prior to the start of the shell growth stage. It can be readily seen that increasing temperatures resulted in higher $\lambda_{1S-1S}$ and larger HWHM, i.e., larger and more polydisperse InP QDs.

Table 5 presents the core growth conditions for each of the four samples, as well as the position and HWHM of the first excitonic peak before the shell growth. These two parameters enabled the calculation of the core diameter and respective size dispersion, which are also presented in Table 5.

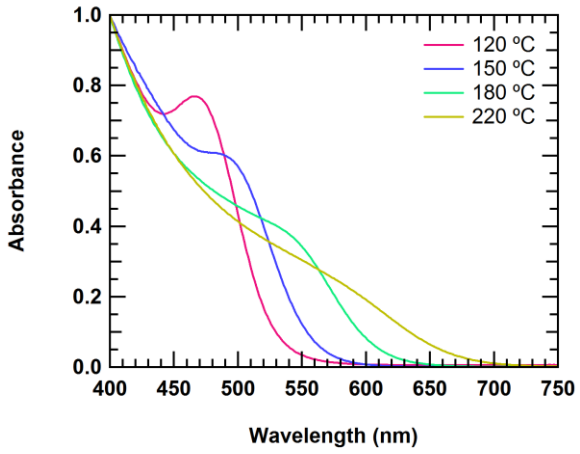


Figure 18. Absorption spectra of aliquots collected before the injection of TOPS during the synthesis of InP/CdS QDs. The spectra were normalised at 400 nm.

The shell growth of the sample that has $\lambda_{1S-1S}$ at 532 nm, as mentioned in the previous section , consisted of 1 h at 180 ºC followed by 2 h at 220 º C. The procedure for the three other samples was similar, except that the temperature was immediately set to

220 ºC after TOPS was injected. To track the shell growth stage, aliquots were collected from each synthesis and in all the cases the evolution of the absorption spectrum was similar to what had been observed in Figure 15b, with a gradual disappearance of the first excitonic peak. These aliquots showed intense light emission under UV excitation, except the last ones collected during the syntheses of the two largest QDs, since the band-edge emission was located in the NIR region.

Table 5. Core growth conditions, absorption properties of the InP core QDs and PL properties of the core-shell QDs of four samples of InP/CdS.

| | | | | | |
|---|---|---|---|---|---|
| Core growth conditions | Temperature (ºC) | 120 | 150 | 180 | 220 |
| | Time (min) | 60 | 20 | 10 | 3 |
| Absorption properties of the core QDs | $\lambda_{1S-1S}$ (nm) | 469 | 491 | 532 | ~560 |
| | HWHM (nm) | 34 | 38 | 44 | ~60 |
| Diameter and relative size dispersion of the core QDs | $d_{core}$ (nm) | 2.5 | 2.7 | 2.9 | 3.1 |
| | $\sigma_{d_{\mathrm{core}}}$ (%) | 6.3 | 7.1 | 8.3 | 11.1 |
| PL properties of the core-shell QDs | Peak position (nm) | n/a | 660 | 755 | 795 |
| | FWHM (nm) | n/a | 135 | 190 | 200 |
| | FWHM (meV) | n/a | 460 | 460 | 437 |
| | PLQY (%) | n/a | 39 | 37 | 17 |

The emission spectra of the three larger InP/CdS QDs are shown in Figure 19 and summarised in Table 5. The two spectra that have an emission peak in the NIR were obtained, as described above, by matching the partial spectra acquired with a visible detector (500-800 nm) and a NIR detector (700-1300 nm). The intensities in the NIR emission spectra were multiplied by a scaling factor determined by examining the overlap of the two spectra from 700 nm to 800 nm.

By changing the core size, the wavelength of the emission could be tuned from 660 nm to 795 nm, without significantly changing the FWHM (it varied from 437 meV to 460 meV). These high values of the FWHM could possibly be due to a high polydispersity of the QDs or to an intrinsic increase of the linewidth caused by a higher exciton-phonon

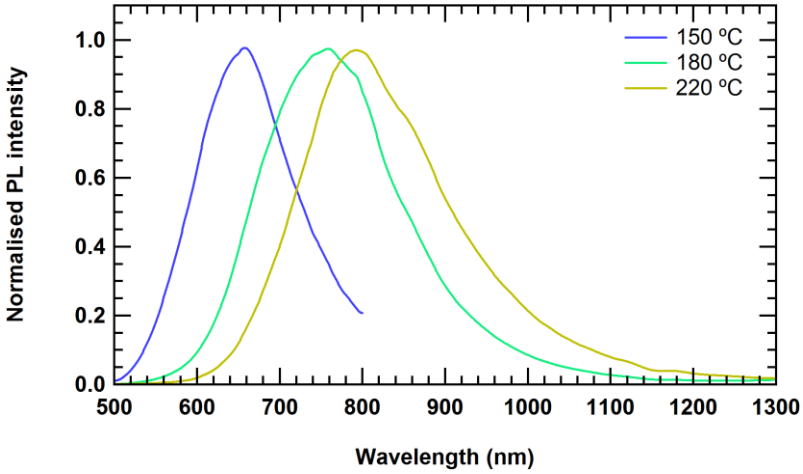

Figure 19. Normalised PL spectra of InP/CdS QDs, excited at 488 nm, with cores grown at different temperatures.

coupling in this type-II structure, as it has been interpreted for quasi-type-II colloidal quantum wells.[49]

The samples emitting at 660 nm and 755 nm presented the highest PLQY, respectively of 39 % and 37 %. The PLQY of the former was slightly underestimated, since the tail of the emission peak above 800 nm was not measured. The bigger and more polydisperse QDs had a considerably lower PLQY of 17 %, which might be a consequence of the formation of a thin CdS shell, since, assuming the same QD concentration, larger cores would need more shell material to achieve the same shell thickness than smaller core QDs. However, this hypothesis would need to be confirmed by analysing the QD size by TEM.

The sample of QDs with $\lambda_{1S-1S}$ at 469 nm, although having a better size dispersion compared to the others, did not present intense PL. This could possibly be due to an insufficient shell growth time, since in this synthesis the shell was only grown for 60 min. Again, this could only be concluded after TEM analysis of the core-shell QDs.

## 4.5. Time-resolved spectroscopic characterization

Time-resolved PL spectroscopy can be employed to measure the electron-hole recombination lifetime of luminescent QDs. The fabrication of type-I or type-II core-shell QDs results in nanostructures with different PL kinetic profiles. While in type-I

heterostructures, like InP/ZnS, the exciton is mainly confined in the core, in type-II QDs like InP/CdS, only the hole is confined in the core whereas the electron is located in the shell.[15] This spatial separation can drastically slow down the radiative decay of an exciton, since the probability of recombination becomes lower. In type-II heterostructures this effect should become more pronounced with an increasing shell thickness, since the electron wavefunction will be spread over a higher shell volume. Therefore, the analysis of the PL decay profile of core-shell QDs can provide some insights on the type of heterostructure. The size of the core also affects the exciton lifetime, as in QDs with larger cores the recombination probability is smaller, resulting in slower lifetime decays.[50] It is thus expected that, for core-shell nanostructures with the same core diameter, InP/CdS QDs show a slower decay rate than InP/ZnS QDs.

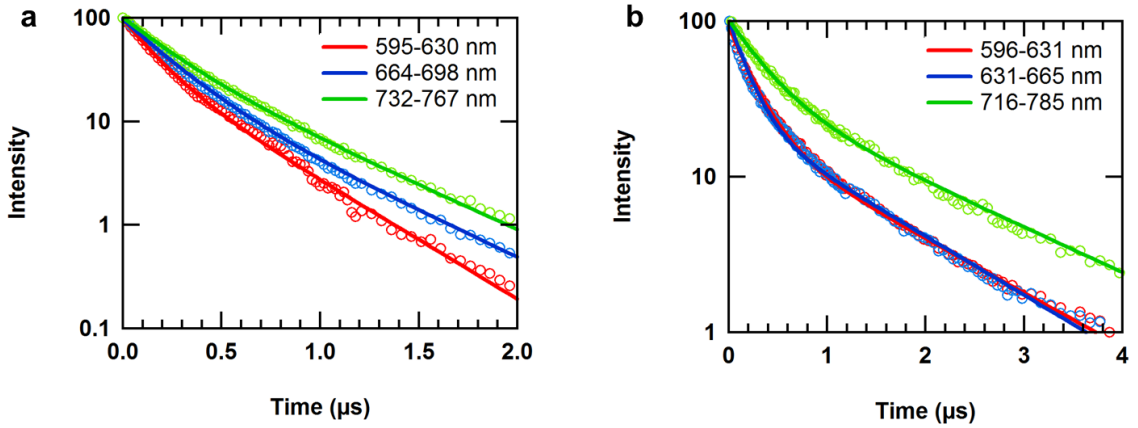


Figure 20. PL decay curves of (a) InP/CdS QDs and (b) InP/ZnS QDs for short (red), intermediate (blue) and long (green) wavelength regions. The solid lines represent the best fit of biexponential decays to the experimental data.

The PL decay of the InP/CdS QDs emitting at 660 nm was analysed and compared with that of a sample of InP/ZnS QDs, with similar emission wavelength and PLQY. The PL spectra were obtained with increasing time delays after pulsed excitation at 465 nm and three wavelength regions were analysed separately to evaluate the dependence of the emission wavelength on the radiative lifetime. Figure 20 presents the PL decay curves of both samples. The experimental data from each decay profile were fitted with a biexponential equation and the lifetime components are described in Table 6.

An approximately linear increase in the average lifetime from shorter to longer wavelengths was observed for InP/CdS QDs, with the fast and the slow components increasing, respectively, from 0.15 μs to 0.22 μs and from 0.38 μs to 0.51 μs. For InP/ZnS QDs (Figure 20b) the PL decay profiles overlapped in the short and intermediate wavelength region, having almost the same average lifetime (0.83 μs and 0.81 μs), while a longer lifetime of 1.1 μs was observed at longer wavelengths, for both faster and slower components.

Table 6. PL lifetime components for InP/CdS and InP/ZnS QDs in different wavelength regions.

| | Wavelength range (nm) | $\tau_1$ (μs) | $\tau_2$ (μs) | $\tau_{average}$ (μs) |
|---|---|---|---|---|
| InP/CdS | 595-630 | 0.15 (62 %) | 0.38 (38 %) | 0.29 |
| | 664-698 | 0.21 (71 %) | 0.49 (29 %) | 0.35 |
| | 732-767 | 0.22 (55 %) | 0.51 (45 %) | 0.41 |
| InP/ZnS | 596-631 | 0.24 (79 %) | 1.25 (21 %) | 0.83 |
| | 631-665 | 0.19 (77 %) | 1.15 (23 %) | 0.81 |
| | 716-785 | 0.35 (66 %) | 1.50 (34 %) | 1.1 |

In fact, the decay rates found for InP/ZnS QDs were slower than those found for InP/CdS, which may be due to a difference in the core QD diameter. The average diameter of the sample of InP/ZnS QDs was 3.2 nm, while the InP/CdS QD diameter was 2.7 nm. Although no information of the shell size could be obtained, this difference in the core diameters, could explain why InP/ZnS QDs presented a longer lifetime than the type-II InP/CdS QDs, since, as mentioned above, shorter decays are expected in QDs with larger core size.

The temporal evolution of the PL spectra after the excitation pulse (Figure 21) could also provide some understanding on the PL phenomena of both QDs. The PL spectra of InP/CdS QDs were shifted to longer wavelengths with increasing delay, which could possibly be explained by a high polydispersity of the core and the shell sizes, since larger QDs would likely show a slower decay than smaller ones, due to a reduced probability of exciton recombination. The PL spectra of InP/ZnS QDs showed the existence of significant trap emission, which could possibly explain the great increase of the lifetime at longer

wavelengths as well as the higher contribution of the slower component in this region (34 %), when compared to shorter wavelengths (21-23 %).

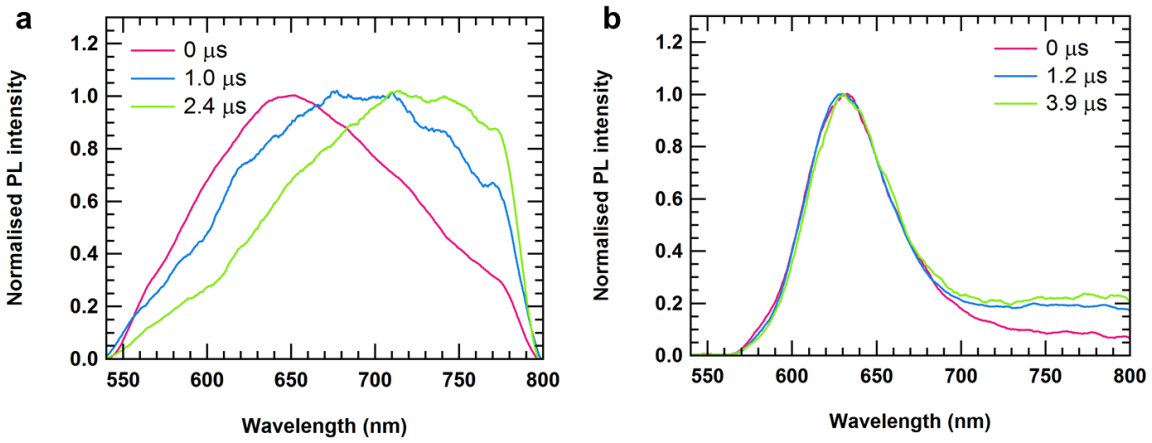


Figure 21. Normalised PL spectra of (a) InP/CdS QDs and (b) InP/ZnS QDs obtained with increasing time delay after pulsed excitation.

However, the radiative decays were slower than those reported in the literature[50] for QDs with similar core size, even in the higher energy region, which cannot be explained by the trap emission. Additional studies should be performed in order to more thoroughly understand this phenomenon, which should include time-resolved PL measurements at cryogenic temperatures, in order to supress potential non-radiative recombination channels generated by phonons.

# Chapter 5. Further research on the synthesis of III-V quantum dots with tris(dimethylamino)phosphine

## 5.1. Introduction

Although InP is the most studied of the III-V systems, others like GaP are also potentially interesting for different applications.[12] The method to synthesize InP QDs described in chapter 4 was cheaper and greener than other previously reported procedures and it would, therefore, be very promising if this method could be extended to the fabrication of other III-V QDs.

Firstly in this chapter, the trial synthesis of GaP QDs based on the hot-injection procedure presented in chapter 4 is discussed. In the second part, some preliminary studies are reported on the reaction mechanism that leads to the formation of InP QDs, which will ultimately enable the fabrication of other III-V materials.

## 5.2. Trial synthesis of GaP QDs

An attempt to synthesize GaP QDs was carried out by adapting the procedure described in section 4.2. In this case, cadmium chloride and TOPS were not used and indium(III) chloride was replaced by gallium(III) chloride. The latter, since it is oxygen sensitive, was mixed with OLA in the glovebox and stirred under heating until a clear solution was obtained, being then injected in a 3-neck flask flushed with nitrogen.

Several experiments were made with the reaction temperatures being varied from 220 ºC to 300 ºC. Figure 22a displays the absorption spectra of the end product of each reaction, 30 min after the injection of $P(DMA)_3$. In all these, a distinctive absorption feature is observed around 370 nm that could be related to the first excitonic transition. However, the position of this absorption feature was temperature-independent, contrarily to what was seen in the absorption spectra of InP QDs, where an increasing temperature resulted in a red shift of the first excitonic peak. Another relevant observation was the

existence of significant light scattering as well as a broad band at longer wavelengths, which was more pronounced with increasing temperature (and had not been observed in the dispersions of InP QDs).

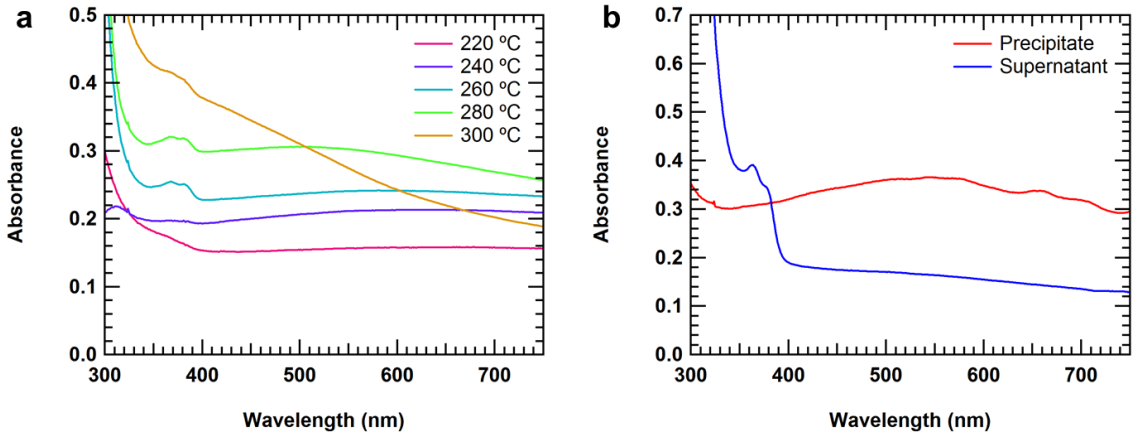


Figure 22. (a) Absorption spectra of the products of the trial syntheses of GaP at different temperatures. The spectra of the reactions at 260 ºC to 300ºC were shifted vertically for clarity. (b) Absorption spectra of the precipitate and supernatant of the reaction carried out at 280 ºC.

The product of the synthesis at 280 ºC was diluted in a small amount of toluene, ethanol was added and the mixture was centrifuged. Figure 22b shows the absorption spectra of the formed precipitate (redispersed in toluene) and the supernatant, where the two absorption features were observed separately: while the peak around 370 nm was seen in the non-polar precipitate, the broad band at longer wavelengths was only detected in the more polar supernatant, thus both appeared to be unrelated.

At 300 ºC, a colour change was detected before the injection of $P(DMA)_3$ and the same experiment was repeated without the addition of this reagent. Figure 23 shows the absorption spectrum of the reaction product where a distinctive peak at 370 nm was observed, similar to those in Figure 22a. This confirmed that the end product of the previous reactions was not GaP as the phosphorus precursor had not been yet added in this case. This sample did not show any scattering or absorption at wavelengths longer than 500 nm, and so this feature, as observed in Figure 22, might be due to the formation of a complex between the phosphorus precursor and OLA or the chloride ions.

Two hypotheses were then raised to possibly explain the obtained results, namely the formation of either gallium nitride or metallic gallium, by reaction with OLA. GaN has

a band gap of 365 nm to 380 nm, depending on its crystal structure,[12] that could be related to the observed absorption peak. The inset in Figure 23 shows the spectrum of the reaction product at shorter wavelengths, obtained after dilution in n-hexane. A peak was detected around 265 nm, which could also be consistent with the formation of metallic gallium nanoparticles, according to previous studies on this nanomaterial.[51]

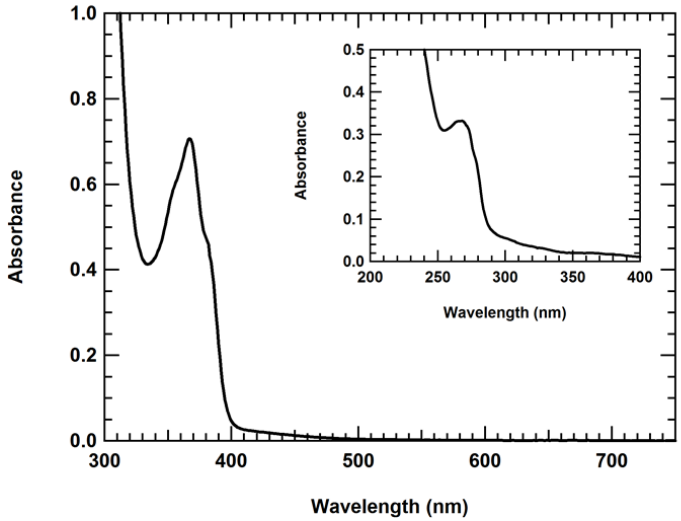


Figure 23. Absorption spectrum of the reacted product of gallium(III) chloride and OLA at 300 ºC. (Inset) Absorption spectrum measured in n-hexane at shorter wavelengths.

The analysis of this sample by XPS showed that gallium was present in three different oxidation states ($Ga^0$, $Ga^I$ and $Ga^{III}$) being the intermediate state the most abundant, which is not consistent with the proposed formation of GaN or metallic gallium, but clearly indicates that gallium(III) was partly reduced.

To fully understand the obtained results, further analysis would be required on the products formed during these reactions. However, this was out of the focus of the aimed research, which was the synthesis of GaP QDs.

## 5.3. Mechanistic studies

As the synthesis of GaP QDs revealed to be more complicated than it was first thought, this research focused instead on trying to understand the reaction mechanism that leads to the formation of InP QDs, since this would enable a better control over the

synthesis products and would be potentially relevant for the fabrication of QDs consisting of other III-V semiconductors, like GaP.

A major difference from the synthesis procedures of chapters 3 and 4 is the use, respectively, of $P(TMS)_3$ and $P(DMA)_3$ (Figure 24). The former has been extensively used as a phosphorus precursor in the synthesis of InP QDs and several studies have been made on this reaction mechanism.[7, 52] On the contrary, the colloidal synthesis of InP using $P(DMA)_3$ was only very recently reported[44] and the synthesis mechanism is still unknown.

These two compounds differ significantly as, in the former, the oxidation state of phosphorus is –3, as it is bound to silicon, which is less electronegative. On the other hand, in the latter, phosphorus is bound to nitrogen, the third most electronegative element in the periodic table, and thus its oxidation state is +3.

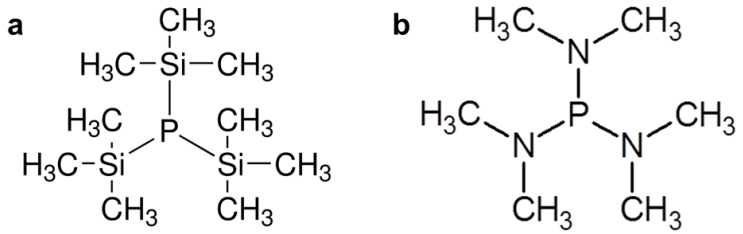


Figure 24. Structure of the two phosphorus precursors: (a) tris(trimethylsilyl)phosphine, $P(TMS)_3$, and (b) tris(dimethylamino)phosphine, $P(DMA)_3$.

Two reasonable pathways for the formation of InP from indium(III) chloride, $P(DMA)_3$ and OLA could be i) the reduction of $In^{III}$ to $In^0$ followed by reaction with $P^{III}$ or ii) the reduction of phosphorus from the oxidation state +3 to –3 and reaction with $In^{III}$. The reduction of either $In^{III}$ or $P^{III}$ could possibly be triggered by the presence of OLA, which has acted as reducing agent in reported synthesis of metal[53-55] and metal oxide[56] nanoparticles. The XPS analysis reported above of a sample of gallium(III) chloride and OLA is in agreement with the first proposed hypothesis, since it revealed that gallium was reduced and a peak possibly corresponding to nitrogen in a higher oxidation state was observed, suggesting a reduction of $Ga^{III}$ by OLA.

To confirm the key role of the amine in the synthesis of InP QDs, a reaction was tried where OLA was replaced by ODE (which is used as solvent in the synthesis with $P(TMS)_3$), and this did not result in the formation of InP. Other primary aliphatic amines like dodecylamine and hexadecylamine were tested and both yielded InP QDs, which

suggested that the double bond of OLA does not play a significant role in the reaction. On the other hand, the reaction with a tertiary amine, namely trioctylamine, did not form InP, which supported the proposed role of the amine as a reducing agent.

Since an NMR analysis of the reaction mixture would possibly provide a useful insight on the synthesis products, the fabrication of InP QDs was also attempted with short-chain amines, as the long chains of fatty amines originate broad resonances that sometimes overlap other relevant but less intense resonances. Thus, the synthesis was tried with butylamine and hexylamine. InP QDs were not obtained with the former, possibly because it has a very low boiling point (78 ºC) and, as the reaction had to be carried out below this temperature, this was not sufficient to overcome the reaction activation energy. Although more slowly than when using OLA, the reaction with hexylamine at 120 ºC seemed to have worked, resulting in a broad absorption feature 60 min after the injection of $P(DMA)_3$ that could indicate the formation of polydisperse InP QDs (Figure 25). Benzylamine has only one aliphatic carbon and would therefore be very suitable for NMR studies, however the synthesis of InP with this amine was not successful either.

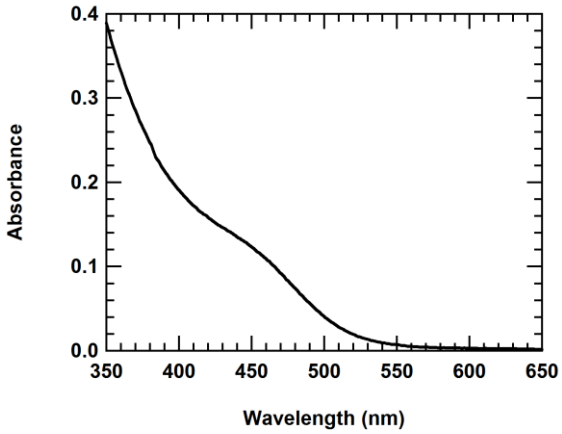


Figure 25. Absorption spectra of the trial synthesis of InP at 120 ºC using hexylamine.

To identify the possible release of gases during the reaction, a gas trap consisting of an aqueous solution of copper sulphate was used. The formation of a pale blue precipitate in the gas trap was observed during a normal synthesis using indium(III) chloride, $P(DMA)_3$ and OLA, which indicated that a basic gas was released, leading to the precipitation of copper hydroxide. This was also detected when $P(DMA)_3$ was injected in

OLA at the same temperature (without indium(III) chloride), suggesting that the gas release resulted from a reaction between $P(DMA)_3$ and OLA.

To identify the gas that was released during this reaction, the same experiment was repeated and the gases were captured in a mixture of hydrochloric acid and methanol. The solution was then evaporated and recrystallized in ethyl acetate and this enabled the identification by XRD of the released gas as being dimethylamine. The formation of this compound when $P(DMA)_3$ and OLA were mixed is a strong indication of the occurrence of an amine exchange process between the dimethylamino groups and the molecules of OLA, as described in equation ( 16 ). In this equation, $P(DMA)_3$ and OLA are represented by their condensed molecular formulas, to denote the proton exchange from OLA to dimethylamine. Since the latter has a boiling point of only 7 ºC it readily evaporates when it is exchanged with OLA.

$$P(N(CH_3)_2)_3 + n\,NH_2C_{18}H_{35} \longrightarrow P(N(CH_3)_2)_{3-n}(NHC_{18}H_{35})_n + n\,NH(CH_3)_2 \qquad (16)$$

To achieve a better understanding on how the amine exchange occurred, the reaction products between $P(DMA)_3$ and an amine were analysed by $^1H$ NMR. As mentioned above, shorter chain amines work better for this analysis and so $P(DMA)_3$ was injected in hexylamine at 120 ºC in a 1:3 ratio and reacted for 90 min. An NMR spectrum (Figure 26) from the final product was obtained, as well as from the pure hexylamine and $P(DMA)_3$. In the spectrum of $P(DMA)_3$ a sharp and very intense doublet at 2.498 ppm was observed, correspondent to the methyl groups coupling with $^{31}P$ nuclei. This resonance is very clear and distinctive from this molecule and thus can be used to follow the exchange process. It could be seen that in the presented reaction, the amine exchange was not complete, as this resonance was still present in the spectrum of the end product. The chemical shift of this resonance, as well as of some of the resonances of hexylamine, was slightly shifted which also indicated that hexylamine and $P(DMA)_3$ had reacted.

This preliminary study confirmed that NMR is a good technique to investigate the exchange process that occurs during the synthesis of InP QDs. A more detailed analysis has to be made in order to fully understand this process and, thereafter, understand how it affects the synthesis of InP.

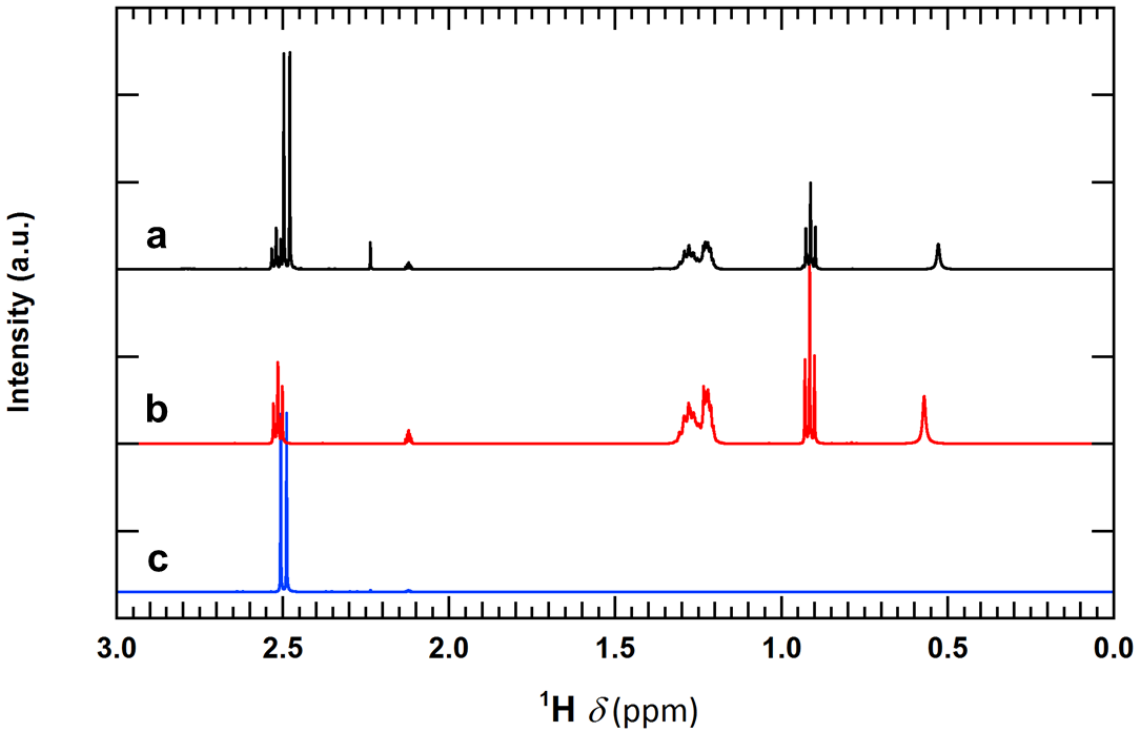


Figure 26. $^1$H NMR spectra of (a) the reaction product of $P(DMA)_3$ and hexylamine at 120 ºC, (b) hexylamine and (c) $P(DMA)_3$ in toluene-d8.

# Chapter 6. Conclusion

The purpose of this thesis was to study the optical properties of InP quantum dots (QDs) and to explore a new method for the synthesis of InP-based nanostructures, specifically InP/CdS QDs. In this chapter, the major findings of this research are highlighted, and their relevance, implications and limitations on this field are discussed. At the end, some suggestions and prospects on future research are presented.

First, InP QDs were synthesized using a hot-injection method with tris(trimethyl-silyl)phosphine as the phosphorus precursor and characterized by ultraviolet-visible absorption spectroscopy, X-ray diffraction (XRD), transmission electron microscopy (TEM) and proton nuclear magnetic resonance (NMR). The synthesized QDs are fairly monodisperse and spherical, have a zinc blende structure and show a first excitonic absorption peak ranging from 520 nm to 620 nm, depending on the QD size. A study of the QD surface enabled the quantitative analysis of the organic ligand shell, which is composed of myristic acid and oleylamine in a ratio of 6.7 to 1.

The absorption spectra and the TEM micrographs were combined to establish a sizing curve that relates the band gap energy to the QD diameter. The determined diameters vary between 2.9 nm and 4.4 nm, corresponding to band gap energies between 1.7 eV and 2.5 eV, and the sizing curve should not be used outside of this range, as that may result in an inaccurate estimation of the QD diameter. Nevertheless, the range of the established sizing curve comprises a large extent of the visible spectrum, making it very useful for a rapid and straightforward determination of the QD diameter from the absorption spectrum of a QD dispersion.

Elemental analysis by inductively coupled plasma optical emission spectrometry and Rutherford backscattering spectrometry, together with the absorption spectra of the synthesized samples, enabled the determination of the intrinsic absorption coefficient $\mu_i$. At 335 nm and 410 nm, we obtained largely size independent average values for $\mu_i$, respectively $(3.22\pm0.10)\times10^5$ cm$^{-1}$ and $(0.920\pm0.030)\times10^5$ cm$^{-1}$, with a mismatch of 23 % and 14 % from the correspondent theoretical $\mu_{i,th}$ values for bulk InP. Out of the diameter range of the studied QDs these values should be carefully utilised since, on the one hand,

QDs with smaller diameters will likely have their excitonic absorption close to 410 nm and, thus, $\mu_i$ will not be size independent in this region. On the other hand, bulk InP reveals a particular absorption feature from 280 nm to 400 nm and larger QDs can possibly show a similar size dependent feature in this wavelength region. If this trait is present in the absorption spectrum of large QDs, $\mu_i$ at 335 nm will not be size independent. Cubic power laws are verified between the molar extinction coefficients $\varepsilon$ at 335 nm and 410 nm, obtained from $\mu_i$, and the QD diameter.

The analysis of these optical properties can find applications, for instance, in the characterization of QD dispersions or in kinetic studies of QD synthesis, as they enable a direct determination of several parameters like the QD diameter, the size dispersion, the QD concentration or the chemical yield from the absorption spectrum of any QD dispersion.

Recently, a cheaper and more sustainable method for the one-pot synthesis of InP/ZnS QDs was described. In this thesis we reported the applicability of this new procedure to the one-pot synthesis of InP/CdS QDs, by adjusting the reaction conditions and replacing the zinc chloride precursor by cadmium chloride and the sulfur precursor (1-dodecanethiol) by the more efficient tri-n-octylphosphine sulphide. Two batches of InP/CdS QDs and InP/ZnS QDs were synthesized and comparatively characterized by XRD and absorption and photoluminescence (PL) spectroscopy.

We report the formation of a type-II nanoheterostructure of InP/CdS with zinc blende core and wurtzite shell. The absorption spectra reveal that the shell growth is accompanied by a gradual disappearance of the first excitonic peak of the core InP, which confirms the fabrication of type-II core-shell QDs, in which there is only a small overlap of the hole and the electron wavefunctions. The PL spectra exhibit highly luminescent band--edge emission of InP/CdS, with broad PL peaks, and no trap emission. Contrariwise, InP/ZnS QDs synthesized in the same conditions show significant trap emission and a five times lower photoluminescence quantum yield (PLQY).

The position of the PL peak of InP/CdS QDs was tuned from 660 nm to 795 nm by varying the temperature of the core growth, with higher temperatures yielding larger and more polydisperse core QDs. The maximum PLQY reached was 39 % and the FWHM of the PL peaks were around 450 meV for all the different samples of the luminescent QDs.

These broad linewidths can possibly be due to a high polydispersity of the QDs or more likely to a higher exciton-phonon coupling in this type-II structure.

Time-resolved PL measurements of InP/CdS and InP/ZnS QDs were performed, where three wavelength regions were analysed. InP/CdS QDs present an approximately linear increase in the average lifetime from shorter to longer wavelengths, ranging between 0.29 μs and 0.41 μs. The temporal evolution of the PL spectra after the excitation pulse shows a red shift of the emission peak, which can be due to the polydispersity of the core and the shell sizes, since larger QDs have a slower decay, compared to smaller ones. The decay profiles of InP/ZnS QDs overlap at short and intermediate wavelengths, with averages lifetimes of 0.82 μs, while at longer wavelengths a longer lifetime of 1.14 μs is observed, due to the existence of significant trap emission.

Although a basic characterization of both QD dispersions was obtained, a more interesting comparison between type-I and type-II structures cannot be established, as the average core diameters of the two are different. A relevant comparison between the PL decay profiles of type-I and type-II core-shell nanostructures can only be made with QD dispersions that have similar core sizes and PLQYs and well passivated surfaces by the shell material, avoiding trap emission.

The reported procedure for the formation of the core-shell QDs comprises great advantages, including economic and environmental benefits, regarding the synthesis of the InP cores, compared to other preceding and more extensively used methods. Hence, it will be very promising if this procedure can be extended to enable the synthesis of other III-V semiconductor QDs. We tried to employ this method to synthesize GaP QDs, although unsuccessfully. Nevertheless, this attempt launched an initial exploratory study on the mechanism of the synthesis of InP QDs with this method. We discovered that oleylamine plays a key role not only as weakly coordinating solvent but probably also as a reducing agent of indium(III) and as an exchange amine with the dimethylamino groups from the phosphorus precursor. This exchange process was studied with a preliminary NMR analysis, which proved to be a good technique to investigate it. A thorough understanding of the reaction mechanism will potentially enable the synthesis of other III-V QD semiconductors, like GaP and InAs.

## 6.1. Future prospects

Although the synthesis of much smaller or much larger InP QDs is rather challenging with the currently used methods, it would be interesting to examine the optical properties of InP out of the studied range. This would enable the establishment of the sizing curve in a broader band gap energy range and the analysis of the size dependence of the optical properties in the high energy region of the absorption spectrum for QDs smaller than 2.9 nm or larger than 4.4 nm. In our study, the indium-to-phosphorus ratio $R_{In/P}$ was determined for only one of the QD dispersions and assumed to be the same for the others. However, this may not be completely true as the QD non-stoichiometry is generally related to the ionic surface shell of the QDs, and $R_{In/P}$ is dependent on the surface area, i.e., on the QD size. Hence, the size dependence of this ratio can be studied by determining $R_{In/P}$ for several QD dispersions with different QD sizes.

Regarding the synthesis of InP/CdS discussed in chapter 4, further characterization of the synthesized QDs should be performed by TEM. This would enable the inspection of the QD morphology and structure, and the estimation of the CdS shell thickness. The fabrication of thicker shells, which would, in principle, yield more stable QDs with an increased emission red shift, can be attempted by several techniques, one of the most simple probably being the multiple injection of cadmium and sulfur precursors, maintaining a one-pot synthesis approach. The analysis of these QDs by NMR, as in chapter 3, would permit a study of their surface capping ligands.

A strategy to tune the emission wavelength of InP/CdS QDs, while keeping low size dispersions, should be investigated, as we found that the size dispersion increases with the temperature of the core growth. Furthermore, single particle spectroscopy can be useful to verify if the large linewidth of the PL peaks is indeed related to a high polydispersity of the QDs or is intrinsic to this material. Moreover, this technique can also be used to study the blinking behaviour of InP/CdS QDs. To obtain a significant comparison between the PL decay kinetics of type-I InP/ZnS and type-II InP/CdS QDs, time-resolved PL measurements should be performed with samples having similar core sizes and PLQYs and without trap emission.

In order to rationally extend the synthesis of InP QDs using tris(dimethyl-amino)phosphine ($P(DMA)_3$) to other III-V QDs, a thorough comprehension of the synthesis mechanism should be acquired. It is necessary to fully understand how does each reagent intervene in the synthesis. Based on the obtained results, the next steps on this process could be the in-depth study of the reaction of the amine with indium(III) chloride and with $P(DMA)_3$ to analyse the metal reduction and the amine exchange, respectively.

In the future, III-V semiconductor QDs, like InP, can potentially replace the widely used II-VI and IV-VI QDs for a huge range of applications, especially due to their low toxicity and high versatility. The ongoing research on these materials should be continued to develop better synthesis strategies and further improve their properties.

# Bibliography


1. ASTM Standard E2456, 2006 (2012), "Standard Terminology Relating to Nanotechnology," ASTM International, West Conshohocken, PA, **2012**, DOI: 10.1520/E2456-06R12, www.astm.org.
2. Alivisatos, A. P., Perspectives on the Physical Chemistry of Semiconductor Nanocrystals. *The Journal of Physical Chemistry* **1996**.
3. Jamieson, T.; Bakhshi, R.; Petrova, D.; Pocock, R.; Imani, M.; Seifalian, A. M., Biological applications of quantum dots. *Biomaterials* **2007,** *28* (31), 4717-4732.
4. Saxl, O. What is Nanotechnology? A guide. *NANO Magazine* [Online], **2014**. www.nanomagazine.co.uk (accessed June 2014).
5. Donegá, C. d. M., Synthesis and properties of colloidal heteronanocrystals. *Chemical Society reviews* **2011,** *40* (3), 1512-1546.
6. Lambert, K. Synthesis and Self-Assembly of Colloidal Quantum Dots. University of Ghent, Ghent, **2011**.
7. Mushonga, P.; Onani, M. O.; Madiehe, A. M.; Meyer, M., Indium Phosphide-Based Semiconductor Nanocrystals and Their Applications. *Journal of Nanomaterials* **2012,** *2012*.
8. Smyder, J. A.; Krauss, T. D., Coming attractions for semiconductor quantum dots. *Materials Today* **2011,** *14*.
9. Sigma Aldrich Co. Lumidots: Quantum Dot Nanocrystals. www.sigmaaldrich.com/materials-science/nanomaterials/lumidots.html (accessed June 2014).
10. Nanocrystals in their prime. *Nature nanotechnology* **2014,** *9* (5), 325.
11. Park, J.; Joo, J.; Kwon, S. G.; Jang, Y.; Hyeon, T., Synthesis of monodisperse spherical nanocrystals. *Angewandte Chemie (International ed. in English)* **2007,** *46* (25), 4630-4660.
12. Fan, G.; Wang, C.; Fang, J., Solution-based synthesis of III–V quantum dots and their applications in gas sensing and bio-imaging. *Nano Today* **2014**.
13. Murray, C. B.; Norris, D. J.; Bawendi, M. G., Synthesis and characterization of nearly monodisperse CdE (E = sulfur, selenium, tellurium) semiconductor nanocrystallites. *Journal of the American Chemical Society* **1993**.
14. Abe, S.; Čapek, R.; De Geyter, B.; Hens, Z., Tuning the postfocused size of colloidal nanocrystals by the reaction rate: from theory to application. *ACS nano* **2012,** *6* (1), 42-53.
15. Reiss, P.; Protière, M.; Li, L., Core/Shell semiconductor nanocrystals. *Small* **2009**.
16. Haubold, S.; Haase, M.; Kornowski, A.; Weller, H., Strongly Luminescent InP/ZnS Core-Shell Nanoparticles. *ChemPhysChem* **2001,** *2*.
17. Dennis, A. M.; Mangum, B. D.; Piryatinski, A.; Park, Y.-S. S.; Hannah, D. C.; Casson, J. L.; Williams, D. J.; Schaller, R. D.; Htoon, H.; Hollingsworth, J. A., Suppressed blinking and auger recombination in near-infrared type-II InP/CdS nanocrystal quantum dots. *Nano letters* **2012,** *12* (11), 5545-5551.
18. Xie, R.; Battaglia, D.; Peng, X., Colloidal InP nanocrystals as efficient emitters covering blue to near-infrared. *Journal of the American Chemical Society* **2007,** *129* (50), 15432-15433.

19. Guzelian, A. A.; Katari, J. E. B.; Kadavanich, A. V.; Banin, U.; Hamad, K.; Juban, E.; Alivisatos, A. P.; Wolters, R. H.; Arnold, C. C.; Heath, J. R., Synthesis of Size-Selected, Surface-Passivated InP Nanocrystals. *The Journal of Physical Chemistry* **1996,** *100*.
20. Micic, O. I.; Curtis, C. J.; Jones, K. M.; Sprague, J. R.; Nozik, A. J., Synthesis and Characterization of InP Quantum Dots. *The Journal of Physical Chemistry* **1994,** *98*.
21. Xu, S.; Kumar, S.; Nann, T., Rapid synthesis of high-quality InP nanocrystals. *Journal of the American Chemical Society* **2006,** *128* (4), 1054-1055.
22. Xu, S.; Ziegler, J.; Nann, T., Rapid synthesis of highly luminescent InP and InP/ZnS nanocrystals. *Journal of Materials Chemistry* **2008,** *18*.
23. Li, L.; Reiss, P., One-pot synthesis of highly luminescent InP/ZnS nanocrystals without precursor injection. *Journal of the American Chemical Society* **2008**.
24. Xie, R.; Li, Z.; Peng, X., Nucleation kinetics vs chemical kinetics in the initial formation of semiconductor nanocrystals. *Journal of the American Chemical Society* **2009,** *131* (42), 15457-15466.
25. Mutlugun, E.; Hernandez-Martinez, P. L.; Eroglu, C.; Coskun, Y.; Erdem, T.; Sharma, V. K.; Unal, E.; Panda, S. K.; Hickey, S. G.; Gaponik, N.; Eychmüller, A.; Demir, H. V., Large-area (over 50 cm × 50 cm) freestanding films of colloidal InP/ZnS quantum dots. *Nano letters* **2012,** *12* (8), 3986-3993.
26. Talapin, D. V.; Gaponik, N.; Borchert, H.; Rogach, A. L.; Haase, M.; Weller, H., Etching of Colloidal InP Nanocrystals with Fluorides: Photochemical Nature of the Process Resulting in High Photoluminescence Efficiency. *The Journal of Physical Chemistry B* **2002,** *106*.
27. Lucey, D. W.; MacRae, D. J.; Furis, M.; Sahoo, Y.; Cartwright, A. N.; Prasad, P. N., Monodispersed InP Quantum Dots Prepared by Colloidal Chemistry in a Noncoordinating Solvent. *Chemistry of Materials* **2005,** *17*.
28. Hens, Z.; Martins, J. C., A Solution NMR Toolbox for Characterizing the Surface Chemistry of Colloidal Nanocrystals. *Chemistry of Materials* **2013**.
29. Mooney, J.; Kambhampati, P., Get the Basics Right: Jacobian Conversion of Wavelength and Energy Scales for Quantitative Analysis of Emission Spectra. *The Journal of Physical Chemistry Letters* **2013,** *4* (19), 3316-3318.
30. Fischer, M.; Georges, J., Fluorescence quantum yield of rhodamine 6G in ethanol as a function of concentration using thermal lens spectrometry. *Chemical Physics Letters* **1996**.
31. Kamal, J. S.; Omari, A.; Van Hoecke, K.; Zhao, Q.; Vantomme, A.; Vanhaecke, F.; Čapek, R. K.; Hens, Z., Size-Dependent Optical Properties of Zinc Blende Cadmium Telluride Quantum Dots. *The Journal of Physical Chemistry C* **2012,** *116*.
32. Jasinski, J.; Leppert, V.; Lam, S.-T.; Gibson, G.; Yang, C.; Zhou, Z.-L., Rapid oxidation of InP nanoparticles in air. *Solid state communications* **2007,** *141* (11), 624-627.
33. Hassinen, A.; Moreels, I.; De Nolf, K.; Smet, P.; Martins, J.; Hens, Z., Short-chain alcohols strip X-type ligands and quench the luminescence of PbSe and CdSe quantum dots, acetonitrile does not. *Journal of the American Chemical Society* **2012,** *134* (51), 20705-20712.
34. Moreels, I.; Lambert, K.; De Muynck, D.; Vanhaecke, F.; Poelman, D.; Martins, J. C.; Allan, G.; Hens, Z., Composition and Size-Dependent Extinction Coefficient of Colloidal PbSe Quantum Dots. *Chemistry of Materials* **2007,** *19*.
35. Morris-Cohen, A. J.; Donakowski, M. D.; Knowles, K. E.; Weiss, E. A., The Effect of a Common Purification Procedure on the Chemical Composition of the Surfaces of

CdSe Quantum Dots Synthesized with Trioctylphosphine Oxide. *The Journal of Physical Chemistry C* **2010,** *114*.
36. Mićić, O. I.; Ahrenkiel, S. P.; Nozik, A. J., Synthesis of extremely small InP quantum dots and electronic coupling in their disordered solid films. *Applied Physics Letters* **2001,** *78*.
37. Hens, Z.; Moreels, I., Light absorption by colloidal semiconductor quantum dots. *Journal of Materials Chemistry* **2012,** *22*.
38. Čapek, R. K.; Moreels, I.; Lambert, K.; De Muynck, D.; Zhao, Q.; Van Tomme, A.; Vanhaecke, F.; Hens, Z., Optical Properties of Zincblende Cadmium Selenide Quantum Dots. *The Journal of Physical Chemistry C* **2010,** *114*.
39. Moreels, I.; Lambert, K.; Smeets, D.; De Muynck, D.; Nollet, T.; Martins, J.; Vanhaecke, F.; Vantomme, A.; Delerue, C.; Allan, G.; Hens, Z., Size-dependent optical properties of colloidal PbS quantum dots. *ACS nano* **2009,** *3* (10), 3023-3030.
40. Aspnes, D.; Studna, A., Dielectric functions and optical parameters of Si, Ge, GaP, GaAs, GaSb, InP, InAs, and InSb from 1.5 to 6.0 eV. *Physical Review B* **1983,** *27*.
41. Bang, K. Y.; Lee, S.; Oh, H.; An, I.; Lee, H., Determination of the optical functions of various liquids by rotating compensator multichannel spectroscopic ellipsometry. *Bulletin of the Korean Chemical Society* **2005,** *26* (6), 947.
42. Chelikowsky, J. R.; Cohen, M. L., Nonlocal pseudopotential calculations for the electronic structure of eleven diamond and zinc-blende semiconductors. *Physical Review B* **1976,** *14* (2), 556-582.
43. Abe, S.; Capek, R.; De Geyter, B.; Hens, Z., Reaction chemistry/nanocrystal property relations in the hot injection synthesis, the role of the solute solubility. *ACS nano* **2013,** *7* (2), 943-949.
44. Song, W.-S.; Lee, H.-S.; Lee, J. C.; Jang, D. S.; Choi, Y.; Choi, M.; Yang, H., Amine-derived synthetic approach to color-tunable InP/ZnS quantum dots with high fluorescent qualities. *Journal of Nanoparticle Research* **2013,** *15*.
45. Lo, S. S.; Mirkovic, T.; Chuang, C.-H.; Burda, C.; Scholes, G. D., Emergent Properties Resulting from Type-II Band Alignment in Semiconductor Nanoheterostructures. *Advanced Materials* **2011**.
46. Wang, J.; Han, H., Hydrothermal synthesis of high-quality type-II CdTe/CdSe quantum dots with near-infrared fluorescence. *Journal of Colloid and Interface Science* **2010**.
47. Yeh, C.-Y.; Lu, Z.; Froyen, S.; Zunger, A., Zinc-blende–wurtzite polytypism in semiconductors. *Physical Review B* **1992**.
48. Shay, J. L.; Wagner, S.; Bachmann, K. J.; Buehler, E., Preparation and properties of InP/CdS solar cells. *Journal of Applied Physics* **2008,** *47* (2), 614-618.
49. Tessier, M. D.; Mahler, B.; Nadal, B.; Heuclin, H.; Pedetti, S.; Dubertret, B., Spectroscopy of colloidal semiconductor core/shell nanoplatelets with high quantum yield. *Nano letters* **2013**.
50. Li, C.; Ando, M.; Enomoto, H.; Murase, N., Highly Luminescent Water-Soluble InP/ZnS Nanocrystals Prepared via Reactive Phase Transfer and Photochemical Processing. *The Journal of Physical Chemistry C* **2008,** *112*.
51. Meléndrez, M. F.; Cárdenas, G.; Arbiol, J., Synthesis and characterization of gallium colloidal nanoparticles. *Journal of Colloid and Interface Science* **2010,** *346* (2), 279-287.
52. Gary, D. C.; Cossairt, B. M., Role of Acid in Precursor Conversion During InP Quantum Dot Synthesis. *Chemistry of Materials* **2013,** *25*.

53. Hiramatsu, H.; Osterloh, F. E., A Simple Large-Scale Synthesis of Nearly Monodisperse Gold and Silver Nanoparticles with Adjustable Sizes and with Exchangeable Surfactants. *Chemistry of Materials* **2004**.
54. Chen, M.; Feng, Y.-G.; Wang, X.; Li, T.-C.; Zhang, J.-Y.; Qian, D.-J., Silver Nanoparticles Capped by Oleylamine: Formation, Growth, and Self-Organization. *Langmuir* **2007**.
55. Mazumder, V.; Sun, S., Oleylamine-mediated synthesis of Pd nanoparticles for catalytic formic acid oxidation. *Journal of the American Chemical Society* **2009**.
56. Xu, Z.; Shen, C.; Hou, Y.; Gao, H.; Sun, S., Oleylamine as Both Reducing Agent and Stabilizer in a Facile Synthesis of Magnetite Nanoparticles. *Chemistry of Materials* **2009**.

# Appendix

## Paper: "Size-Dependent Optical Properties of Colloidal Indium Phosphide Quantum Dots"

# Size-Dependent Optical Properties of Colloidal Indium Phosphide Quantum Dots

J. Ministro[a,b], E. Van Harten[a,b], S. Abe[a,b], L. Balcaen[c], Q. Zhao[d], M. D. Tessier[a,b], Z. Hens[a,b]

[a] Physics and Chemistry of Nanostructures, Ghent University, Krijgslaan 281-S3, B-9000 Gent, Belgium, [b] Center for Nano- and Biophotonics, Ghent University, B-9000 Gent, Belgium, [c] Department of Analytical Chemistry, Ghent University, Krijgslaan 281-S12, B-9000 Gent, Belgium, [d] Instituut voor Kern- en Stralingsfysica, K.U.Leuven, Celestijnenlaan 200D, B-3001 Leuven, Belgium

A multitude of research on colloidal quantum dots (QDs) requires detailed knowledge on their optical properties. In this work, we investigate the basic optical properties of InP QDs, determining the relation between the band gap energy and the QD size (sizing curve) and quantifying the intrinsic absorption coefficient and the molar extinction coefficient. The sizing curve was established from the position of the first excitonic absorption peak of QD dispersions and the average diameter, obtained by transmission electron microscopy. The intrinsic absorption and molar extinction coefficients were determined from quantitative elemental analysis and the absorbance of the nanocrystals at short wavelengths. We found that the intrinsic absorption coefficient is size-independent at short wavelengths and the molar extinction coefficient increases linearly with the QD volume. These results provide the means to precisely determine parameters like the QD size and concentration.

## Introduction

Due to their unique optical and electronic properties, colloidal semiconductor nanocrystals or quantum dots (QDs) have been extensively studied in the last decades. High-quality QDs present broad absorption spectra and narrow and symmetrical emission peaks with quantum yields over 80 %. They are also more photostable, have longer excited state lifetimes and cover a wider spectral range than most organic dyes (1). Moreover, due to quantum confinement, their properties become size-dependent and can be tuned based on QD size and shape, rather than only on their composition (2). All these characteristics make QDs very interesting materials for a whole range of applications, from biological imaging to photovoltaic and light-emitting devices (3-5).

Owing to the size dependence of the QD properties, determining the QD diameter $d_{QD}$ and the concentration of semiconductor material in a QD dispersion is essential in colloidal QD research, from the point of view of characterization, post-synthesis procedures or application in technological fields (6). A study of the optical properties of InP QDs is thus essential to (i) establish a sizing curve that relates $d_{QD}$ to the band gap energy $E_g$ and (ii) determine the intrinsic absorption coefficient $\mu_i$ and the molar extinction coefficient $\varepsilon$ that enable the calculation of the concentration of semiconductor material and of QDs in a dispersion, respectively. These properties find application, for instance, in the characterization of QD dispersions or in kinetic studies of QD synthesis,

as they give access to the direct determination of some parameters, such as the size dispersion, the QD concentration and the chemical yield, from the absorption spectrum of any QD dispersion.

In this work, we analyse several InP QD dispersions by UV-vis absorption spectroscopy, transmission electron microscopy and elemental analysis (ICP-OES and RBS) to establish a sizing curve and determine the intrinsic absorption coefficient and molar extinction coefficient of these QDs at short wavelengths.

## Experimental Section

### Chemicals

Methanol (rectapur grade), 2-propanol (rectapur grade), toluene (technical grade), chloroform (normapur grade), acetonitrile (gradient grade) and concentrated (65 %) nitric acid ($HNO_3$, normatom ultrapure) were purchased from VWR BDH Prolabo. Indium(III) acetate (99.99 %) was purchased from Sigma Aldrich. Tris(trimethylsilyl)phosphine ($P(TMS)_3$, 98 %) and oleylamine (OLA, C18-content 80-90 %) were purchased from Acros Organics. 1-octadecene (ODE, technical grade) was purchased from Alfa Aesar. Myristic acid (MA, quality "for synthesis") was purchased from Merck. Deuterated toluene (toluene-d8, 99.96 % deuterated) was purchased from CortecNet.

### QD Synthesis

InP QDs synthesis was based on the method reported by Xie et al. (7). The phosphorus precursor was prepared by mixing 60 µL (0.20 mmol) of $P(TMS)_3$, 735 µL (2.20 mmol) of OLA and 705 µL of ODE in a glovebox under a nitrogen atmosphere. A typical indium precursor was prepared by mixing 117 mg (0.400 mmol) of indium(III) acetate and 388 mg (1.70 mmol) of MA in 5.00 mL of ODE, and heating for 2 h at 120 ºC under vacuum in a Schlenk line.

In a typical synthesis, carried out in the glovebox, the indium precursor was loaded into a 50 mL 3-neck flask and the temperature was raised to 188 ºC. The phosphorus precursor was then rapidly injected into the reaction mixture and the temperature was reduced and maintained at 178 ºC for the growth of the nanocrystals. The reaction was stopped after 1h by temperature quenching with 3 mL of ODE.

The obtained product was diluted in toluene and purified by subsequent cycles of precipitation with a non-solvent mixture, centrifugation for 5 min at 3500 rpm and redispersion in toluene. During the first two purification cycles, a mixture of 2-propanol and methanol was used as non-solvent and, in the following 6 to 8 cycles, 2-propanol and acetonitrile were used. The purified QDs were dispersed in a small amount of toluene and stored in the glovebox.

Different QD sizes were obtained by adding a variable amount of MA (from 1.55 to 1.90 mmol) to prepare the indium precursor used in each synthesis.

### Purity Assessment

$^1$H NMR was used to detect possible traces of indium myristate or free OLA. The NMR samples were dried by evaporating the original solvent and suspending the QDs in toluene-d8. $^1$H NMR measurements were performed at room temperature on a Bruker

500 MHz AVANCE III spectrometer equipped with a 5mm BBI-z or a 5mm TXI-z probe.

Size Determination

The average diameter $d_{QD}$ of the InP QD suspensions was determined from bright field TEM images recorded using a $C_s$ corrected JEOL 2200-FS microscope. The samples were prepared by dropcasting a diluted dispersion of QDs on carbon coated copper grids. The average diameter and the size dispersion were determined by measuring the nanocrystal area of 80 to more than 250 nanocrystals and assuming spherical particles.

Composition and Concentration Determination

ICP-OES was used for the elemental quantification of indium. The QD samples were prepared by drying a known volume of a QD suspension in a nitrogen flow and digesting the dried samples in a known volume of nitric acid. Phosphorus analysis by this technique is unreliable and RBS was used to determine the indium-to-phosphorus ratio, $R_{In/P}$. Samples for RBS analysis consisted of films of InP QDs deposited on a MgO substrate by spincoating. $R_{In/P}$ was obtained from the ratio of the backscattered intensity of $He^{2+}$ ions with In and P nuclei after $Z^2$ correction:

$$R_{InP} = \frac{I_{In}}{I_P}\frac{Z_P^2}{Z_{In}^2} \quad [1]$$

where $I_{In}$ and $I_P$ are the integrals of the peaks corresponding to In and P, respectively, and $Z$ is the atomic number. The measurements were done with an accelerated $He^{2+}$ ion beam and an NEC 5SDH-2 Pelletron tandem accelerator with a semiconductor detector.

Absorbance Measurements

For the absorption measurements, a known volume of InP QDs was diluted 60 to 300 times in chloroform. The absorbance spectrum of the resulting dispersion was recorded with a Perkin-Elmer Lambda 950 UV-vis spectrophotometer.

## Results and Discussion

Structural Characterization

The structural characterization of the synthesized InP QDs was done with XRD and TEM. Figure 1a presents the X-ray diffractogram of the nanoparticles, revealing a crystal structure that matches the reflections of bulk InP with a cubic zinc blende structure. TEM micrographs (Figure 1b) demonstrate that fairly isotropic and uniform nanoparticles were formed, with low size polydispersity.

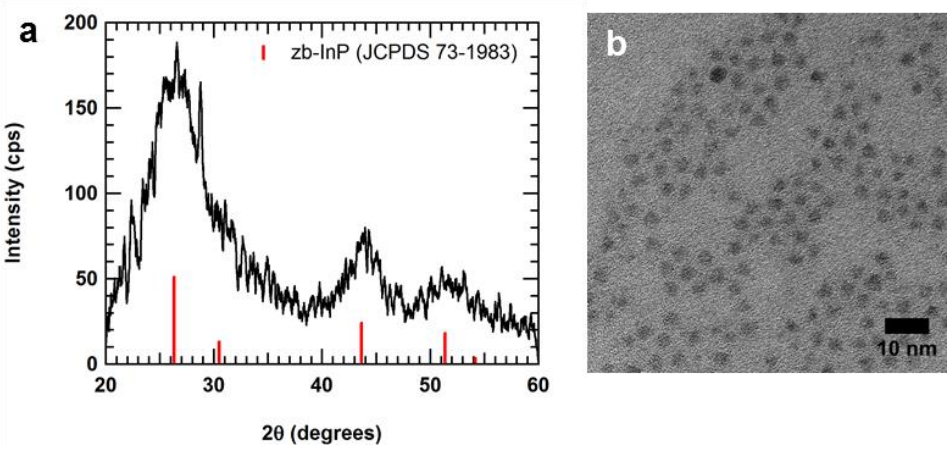


Figure 1. (a) X-ray diffractogram of InP QDs. The vertical red lines indicate the characteristic peak positions of bulk zinc blende InP. (b) TEM images of the synthesized InP QDs.

To quantitatively analyse the amount of indium in the QDs, it is necessary that no other indium-containing species (such as indium myristate) are present in the QD dispersion, in which case the amount of InP is overestimated. The purity of the dispersion was assessed by $^{1}$H NMR spectroscopy (8). Figure 2a shows that, apart from the resonances from toluene and impurities, no sharp signals arising from free species as indium myristate or OLA (which could possibly complex with indium) were present in the QD dispersion. The broad resonances correspond to bound ligands capping the QD surface, mainly deprotonated MA (Figure 2b). Broad proton resonances at 5.60 ppm and 2.65 ppm were attributed to bound OLA ligands (see spectrum of unbound OLA in Figure2c), meaning that OLA was also part of the ligand shell.

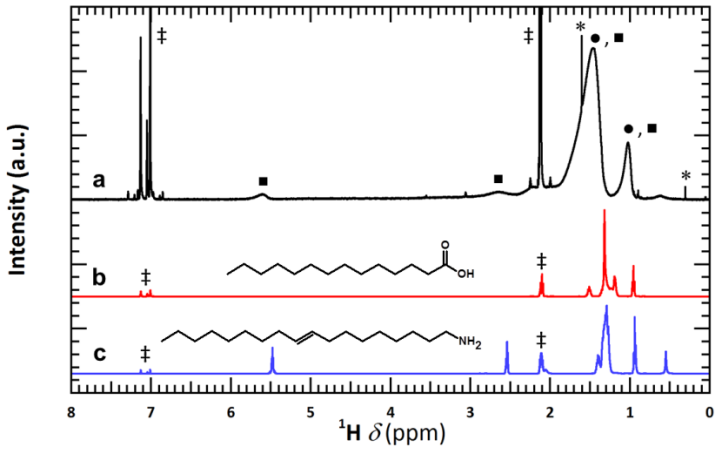


Figure 2. (a) $^{1}$H NMR spectrum of a QD dispersion of InP in toluene d-8 (● and ■ represent the resonances assigned to MA and OLA, respectively). Structure and $^{1}$H NMR spectrum of (b) MA and (c) OLA in toluene-d8. ‡ indicates resonances from solvent and * from impurities.

Sizing Curve

In order to obtain a sizing curve that relates the first excitonic absorption peak maximum $\lambda_{1S-1S}$ to $d_{QD}$, 10 batches of InP QDs were synthesized and purified, with $\lambda_{1S-1S}$ ranging from 521 nm to 619 nm (Figure 3a). Several TEM images of each QD dispersion were obtained, to have a representative sample, and the average diameter was determined.

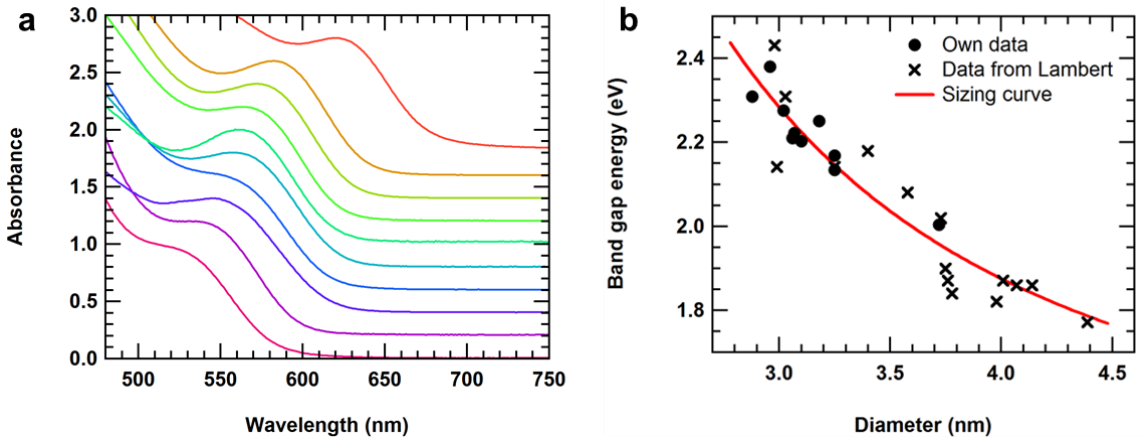


Figure 3. (a) Absorption spectra of 10 batches of differently sized InP QDs from different syntheses, used to construct the sizing curve. The spectra were normalised at $\lambda_{1S-1S}$ and shifted vertically for clarity. (b) Plot of the energy of the first excitonic peak versus the nanoparticle diameter of (circles) synthesized InP QDs and (crosses) InP QDs obtained by Lambert (9). The red line represents the best fit of the experimental data, according to equation [1].

Figure 3b represents the different data points obtained for the band gap energy $E_g$ (in eV) as a function of $d_{QD}$ (in nm). The results from the 10 batches of QDs were used together with those obtained by Lambert (9) to construct the sizing curve and very good agreement between both sets of data was found. The red line in Figure 3b represents the best fit to the experimental data, which was given by the following empirical formula:

$$E_g = 1.35 + \frac{1}{(0.119 \pm 0.003) d_{QD}^2} \quad [1]$$

This sizing curve fits well the data points and is in agreement with the sizing curves determined by other authors (10, 11) and can thus be used to easily and reliably estimate $d_{QD}$ from the absorption spectrum of a dispersion of QDs, in the range of 1.7 eV to 2.5 eV. Band gap energies outside of this interval will be calculated based on an extrapolation from the fit, with additional error on the estimation.

Intrinsic Absorption Coefficient

The intrinsic absorption coefficient $\mu_i$ can be used to determine the concentration of InP in a colloidal dispersion of QDs (12), as it relates the absorbance $A$ to the QD volume fraction $f$ ($L$ is the path length):

$$\mu_i = \frac{A \ln 10}{f L} \quad [2]$$

The volume fraction, which is the volume occupied by the QDs per unit of sample volume, describes the composition of the colloidal dispersion and is given by (6):

$$f = \frac{V_m n_{InP}}{V_{total}} = V_m \frac{C_{In}}{2}\left(1 + \frac{1}{R_{In/P}}\right) \quad [3]$$

where $V_m$ is the molar volume of InP (0.0303 L/mol), $n_{InP}$ is the amount of material, $C_{In}$ is the molar concentration of indium and $R_{In/P}$ is the indium-to-phosphorus ratio.

$\mu_i$ can thus be calculated by combining elemental analysis (to determine $f$) and absorption spectroscopy (to determine $A$). In this study, $C_{In}$ of six batches of differently sized InP QDs was quantified by ICP-OES. RBS was used to determine $R_{In/P}$ of one of the samples and the obtained value was employed as the ratio for the remaining samples.

The absorption spectra of these samples were combined with the $f$ values to calculate $\mu_i$ according to equation [2], and the $\mu_i$ spectra are shown in Figure 4a. Previous studies on the optical properties of other semiconductor nanocrystalline materials (6, 13-14) demonstrated that $\mu_i$ spectra of differently sized QDs coincide at short wavelengths. This trend was observed for InP QDs at wavelengths below 440 nm, especially around 335 nm and 410 nm (Figure 4b and c), where the relative standard deviation from the average value $\bar{\mu}_i$ was smaller (Figure 4d), suggesting that the quantum confinement effects were minimal at these wavelengths.

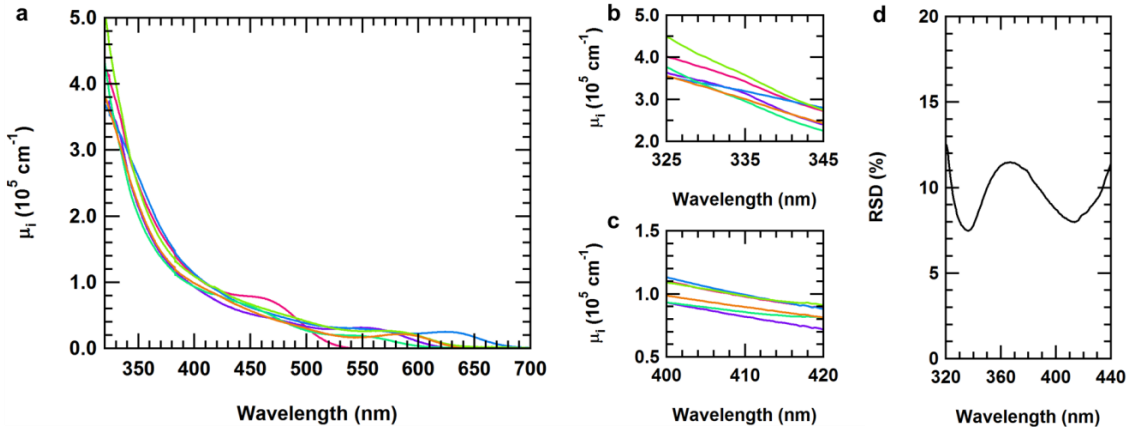


Figure 4. (a) $\mu_i$ spectra of six differently sized samples of InP QDs in chloroform. (b, c) Zoom of (a) in the range 325 nm to 345 nm and 400 nm to 420 nm, respectively. (d) Relative standard deviation on $\mu_i$ as a function of wavelength calculated using the six spectra shown in (a).

**TABLE I.** $\bar{\mu}_i$ for InP in chloroform at 335 nm and 410 nm..

| $\lambda$ (nm) | $\bar{\mu}_i$ ($10^5$ $cm^{-1}$) | $RSD_{\bar{\mu}_i}$ (%) |
|---|---|---|
| 335 | 3.22 | 7.56 |
| 410 | 0.920 | 8.08 |

Table I displays $\bar{\mu}_i$ at 335 nm and 410 nm, as well as the relative standard deviation of the experimental determination. As mentioned, the best overlap for $\mu_i$ of the analysed samples was found around these two wavelengths. Nevertheless, QDs with a diameter below the range of the ones analysed (smaller than around 2.5 nm), can possibly show quantum confinement effects at 410 nm, since their first excitonic transition will have a maximum close to this wavelength. In this case, $\mu_i$ at 410 nm will not be suitable to calculate the concentration of InP and the value at 335 nm should be used instead.

Due to the lack of quantum confinement effects in the higher energy region of the spectra, a good match is usually obtained between $\mu_i$ of QDs and of the bulk material (12, 13). The theoretical $\mu_{i,th}$ can be calculated by using the optical constants for bulk InP (12, 15, 16):

$$\mu_{i,th} = \frac{4\,\pi\,n\,k\,|f_{LF}|^2}{n_s\;\lambda} \qquad [4]$$

where $n$ and $k$ are the real and imaginary parts of the refractive index of bulk InP, $n_s$ is the refractive index of the solvent and $f_{LF}$ is the local field factor, which represents the ratio between the electric field inside and outside of the QD and is given by:

$$|f_{LF}|^2 = \frac{9{n_s}^4}{\left(n^2 - k^2 + 2{n_s}^2\right)^2 + 4(nk)^2} \qquad [5]$$

Figure 5a represents the bulk $\mu_{i,th}$ spectrum of InP in chloroform, calculated from equation [4]. A particular absorption feature is clearly seen in the region 280-400 nm, which is distinct from what is observed in the spectra of the QDs. A similar characteristic was reported by Kamal et al. (6) in the bulk $\mu_{i,th}$ spectrum of CdTe (see inset of Figure 5a) and it was attributed to the transition connecting the initial and final states along the Λ direction in the Brillouin zone (6, 17). This is in agreement with the absence of this feature in the spectra of the QDs, as such transitions would be less pronounced and shifted to higher energy values and thus would not be seen above 320 nm.

The mismatch between bulk and nanocrystalline InP means that quantum confinement effects in the absorption spectra are still present at wavelengths shorter than 400 nm. Although they are not detectable in the $\mu_i$ spectra of the studied QDs, this may not be the case for large QDs with diameters closer to the exciton Bohr diameter. The $\mu_i$ spectrum of such nanocrystals would likely show a similar feature to the bulk $\mu_{i,th}$, as it was observed for large CdTe QDs (red lines in the inset of Figure 5a). In this case, the absorption at wavelengths below 400 nm cannot be used to determine the concentration of InP since, as it is suggested, considerable size effects on $\mu_i$ would be present, and the $\mu_i$ determined at 410 nm may provide a more accurate estimation of the concentration.

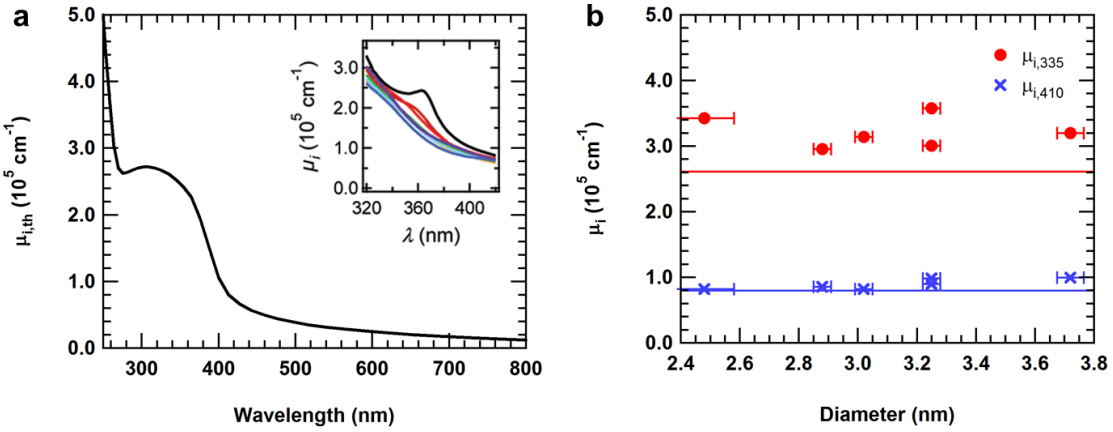


Figure 5. (a) $\mu_{i,th}$ calculated for bulk InP in chloroform. (Inset) $\mu_i$ spectra of CdTe QDs of different sizes and $\mu_{i,th}$ (black line) calculated for bulk CdTe. Reproduced from (6). (b) $\mu_i$ of six samples at 335 nm (red circles) and 410 nm (blue crosses) as a function of $d_{QD}$. The horizontal lines represent $\mu_{i,th}$ at these wavelengths. The error bars of the experimental points represent the standard error of the mean.

As already mentioned, $\mu_i$ values were in good agreement, especially at 335 nm and 410 nm, in the range of diameters of the analysed samples (around 2.5-3.7 nm). Figure 5b shows $\mu_{i,335}$ and $\mu_{i,410}$ as a function of $d_{QD}$, confirming that both values are size--independent. The horizontal lines correspond to $\mu_{i,th}$ at each wavelength and the average experimental values $\bar{\mu}_{i,335}$ and $\bar{\mu}_{i,410}$ are higher than those by 23 % and 14 %, respectively. These differences are not surprising, due to the size effects discussed in this section.

Molar Extinction Coefficient

The molar extinction coefficient $\varepsilon$ for QDs with a given diameter $d_{QD}$ can be calculated from $\mu_i$ as (12):

$$\varepsilon = \frac{\pi d_{QD}^3 N_A}{6 \ln 10} \mu_i \quad [6]$$

where $N_A$ is the Avogadro's number.

Figure 6 presents $\varepsilon_{335}$ and $\varepsilon_{410}$ for the six InP QD samples as a function of $d_{QD}$. The data were fitted to a $d_{QD}^3$ power law (full lines in the figure) and the obtained equations for $\varepsilon_\lambda$ (in $cm^{-1}$ $mol^{-1}$ L) were ($d_{QD}$ is given in nm):

$$\varepsilon_{335} = (4.40 \pm 0.19) \times 10^4 \, d_{QD}^3 \quad [7]$$

$$\varepsilon_{410} = (1.29 \pm 0.06) \times 10^4 \, d_{QD}^3 \quad [8]$$

It can be seen in Figure 6 that, for both wavelengths, $\varepsilon$ scaled well with the QD volume, confirming that the $\bar{\mu}_i$ values found in the previous section are size-independent. A similar trend was found for InP QDs with different ligands and solvents, namely, InP QDs capped with tri-n-octylphosphine oxide and dispersed in n-hexane (18) [26] and InP

QDs capped with and dispersed in pyridine (9). However, different values were obtained for the coefficient in the $d_{QD}^3$ fit (respectively, $3.86\times10^4$ and $3.45\times10^4$ $cm^{-1}$ $mol^{-1}$ L $nm^{-3}$), since the absorbance was measured at 350 nm and different solvents and capping ligands were used.

Equations [7] and [8] are very useful as, together with the sizing curve given in equation [1], they enable the direct determination of the concentration of InP QDs from the absorption spectrum, using the Lambert-Beer law.

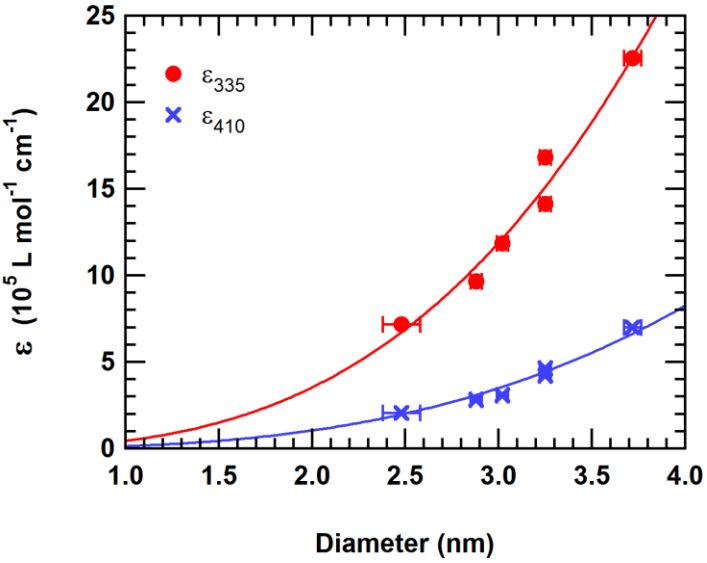


Figure 6. Molar extinction coefficient $\varepsilon$ of 6 samples at 335 nm (red circles) and 410 nm (blue crosses) as a function of $d_{QD}$. The trend lines show the best fit of the data to a $d_{QD}^3$ power law. The error bars of the experimental points represent the standard error of the mean.

## Conclusions

InP QDs were synthesized and structurally characterised. Analysing TEM images, we determined the average diameter of several samples of differently sized QDs to construct a sizing curve that relates the band gap energy (obtained by UV-vis absorption spectroscopy) to the QD diameter. Elemental analysis and absorption spectroscopy enabled the determination of the intrinsic absorption coefficient $\mu_i$ of InP QDs. At 335 nm and 410 nm, we obtained largely size independent average values for $\mu_i$, respectively $(3.22\pm0.10)\times10^5$ $cm^{-1}$ and $(0.920\pm0.030)\times10^5$ $cm^{-1}$, with a mismatch of 23 % and 14 % from the correspondent theoretical $\mu_{i,th}$ values of bulk InP. Cubic power laws were verified between the molar extinction coefficients ε at 335 nm and 410 nm, obtained from $\mu_i$, and the QD diameter.

The analysis of these optical properties can find applications, for instance, in the characterization of QD dispersions or in kinetic studies of QD synthesis, as they enable a direct determination of several parameters like the QD diameter, the size dispersion, the QD concentration or the chemical yield from the absorption spectrum of any QD dispersion.

## Acknowledgements

The authors thank Dr. Karel Lambert for his previous work and results on InP QDs. Ruben Dierick and Kim De Nolf are acknowledged for the XRD and the NMR measurements.

## References

1. P. Mushonga, M. Onani, A. Madiehe and M. Meyer, *J. Nanomater*, **2012** (2012).
2. C. d. M. Donegá, *Chem. Soc. Rev.*, **40**, 1512 (2011).
3. H. Demir, S. Nizamoglu, T. Erdem, E. Mutlugun, N. Gaponik and A. Eychmüller, *Nano Today*, **6** (2011).
4. J. A. Smyder and T. D. Krauss, *Materials Today*, **14** (2011).
5. H. Mattoussi, G. Palui and H. Na, *Adv. Drug Deliver. Rev.*, **64**, 138 (2012).
6. J. S. Kamal, A. Omari, K. Van Hoecke, Q. Zhao, A. Vantomme, F. Vanhaecke, R. K. Čapek and Z. Hens, *J. Phys. Chem.* C, **116** (2012).
7. R. Xie, D. Battaglia and X. Peng, *J. Am. Chem. Soc.*, **129**, 15432 (2007).
8. Z. Hens and J. C. Martins, *Chem. of Mater.* (2013).
9. K. Lambert, *Synthesis and Self-Assembly of Colloidal Quantum Dot'*, University of Ghent, Ghent (2011).
10. A. Guzelian, J. Katari, A. Kadavanich, U. Banin, K. Hamad, E. Juban, A. Alivisatos, R. Wolters, C. Arnold and J. Heath, *J. Phys. Chem.*, **100** (1996).
11. O. I. Mićić, S. P. Ahrenkiel and A. J. Nozik, *Appl. Phys. Lett.*, **78** (2001).
12. Z. Hens and I. Moreels, *J. Mater. Chem.*, **22** (2012).
13. R. K. Čapek, I. Moreels, K. Lambert, D. De Muynck, Q. Zhao, A. Van Tomme, F. Vanhaecke and Z. Hens, *J. Phys. Chem. C*, **114** (2010).
14. I. Moreels, K. Lambert, D. Smeets, D. De Muynck, T. Nollet, J. Martins, F. Vanhaecke, A. Vantomme, C. Delerue, G. Allan and Z. Hens, *ACS nano*, **3**, 3023 (2009).
15. D. Aspnes and A. Studna, *Phys. Rev. B*, **27** (1983).
16. K. Bang, S. Lee, H. Oh, I. An and H. Lee, *Bull. Korean Chem. Soc.*, **26**, 947 (2005).
17. J. R. Chelikowsky and M. L. Cohen, *Phys. Rev. B*, **14**, 556 (1976).